Human Brain Mapping

WILEY

RESEARCH ARTICLE OPEN ACCESS

Advancing Thalamic Nuclei Segmentation: The Impact of Compressed Sensing on MRI Processing

Sebastian Hübner[1] | Stefano Tambalo[1] | Lisa Novello[1,2] | Tom Hilbert[3,4,5] | Tobias Kober[3,4,5] | Jorge Jovicich[1]

[1]Center for Mind/Brain Sciences—CIMeC, University of Trento, Rovereto, Italy | [2]Data Science for Health, Fondazione Bruno Kessler, Trento, Italy | [3]Advanced Clinical Imaging Technology, Siemens Healthineers International AG, Lausanne, Switzerland | [4]Department of Radiology, Lausanne University Hospital and University of Lausanne, Lausanne, Switzerland | [5]Signal Processing Laboratory 5 (LTS5), Ecole Polytechnique Fédérale de Lausanne (EPFL), Lausanne, Switzerland

Correspondence: Sebastian Hübner (sebastian.hubner@unitn.it)

Received: 12 July 2024 | **Revised:** 9 December 2024 | **Accepted:** 13 December 2024

Funding: This work was supported by the Municipality of Rovereto (2022–2024).

Keywords: compressed sensing MRI | fast MRI acquisition | FastSurfer | FreeSurfer | segmentation | thalamic nuclei | volumetric characterization

ABSTRACT

The thalamus is a collection of gray matter nuclei that play a crucial role in sensorimotor processing and modulation of cortical activity. Characterizing thalamic nuclei non-invasively with structural MRI is particularly relevant for patient populations with Parkinson's disease, epilepsy, dementia, and schizophrenia. However, severe head motion in these populations poses a significant challenge for in vivo mapping of thalamic nuclei. Recent advancements have leveraged the compressed sensing (CS) framework to accelerate structural MRI acquisition times in MPRAGE sequence variants, while fast segmentation tools like FastSurfer have reduced processing times in neuroimaging research. In this study, we evaluated thalamic nuclei segmentations derived from six different MPRAGE variants with varying degrees of CS acceleration (from about 9 to about 1-min acquisitions). Thalamic segmentations were initialized from either FastSurfer or FreeSurfer, and the robustness of the thalamic nuclei segmentation tool to different initialization inputs was evaluated. Our findings show minimal sequence effects with no systematic bias, and low volume variability across sequences for the whole thalamus and major thalamic nuclei. Notably, CS-accelerated sequences produced less variable volumes compared to non-CS sequences. Additionally, segmentations of thalamic nuclei initialized from FastSurfer and FreeSurfer were highly comparable. We provide the first evidence supporting that a good segmentation quality of thalamic nuclei with CS T1-weighted image acceleration in a clinical 3T MRI system is possible. Our findings encourage future applications of fast T1-weighted MRI to study deep gray matter. CS-accelerated sequences and rapid segmentation methods are promising tools for future studies aiming to characterize thalamic nuclei in vivo at 3T in both healthy individuals and clinical populations.

1 | Introduction

The thalamus is a diencephalic structure of the mammalian forebrain involved in gating sensorimotor input to the cortex and modulating cortical activity via transthalamic corticocortical pathways (Jones 2007; Sherman 2017). It is composed of a collection of gray matter nuclei, each of which is characterized by specific histological (Jones 2007; Morel 2007; Sherman 2017), connectional (Behrens et al. 2003; Sherman 2017), and functional properties (Herrero, Barcia, and Navarro 2002; Zhang et al. 2008). Individual thalamic nuclei are differently associated with sensorimotor functions (Jones 2007; Sherman 2017) and cognitive processes, such as attention (Grieve, Acuña, and Cudeiro 2000; Guedj and Vuilleumier 2023), memory (Leszczyński and Staudigl 2016; Sweeney-Reed et al. 2021), emotions (Arend, Henik, and Okon-Singer 2015; Golden et al. 2016),

Summary

- MPRAGE variants can be accelerated with compressed sensing without increasing volume variability in the thalamus and major thalamic nuclei.
- Thalamic nuclei segmentations initialized from FastSurfer whole-brain data provide comparable results to FreeSurfer.
- Practitioner key points
  - To assess thalamic nuclei atrophy in clinical populations, faster thalamic nuclei volumetric segmentations can be achieved with both T1w MPRAGE sequences accelerated with compressed sensing, and fast initial segmentations using FastSurfer, with no significant effects on whole thalamus and major thalamic nuclei volumes.

language (Wahl et al. 2008; Hebb and Ojemann 2013), executive functions (Van der Werf et al. 2003; Jakab, Blanc, and Berényi 2012), and consciousness (Schiff 2008; Ward 2011), and are also affected under neurological and psychiatric conditions including, among others, Alzheimer's disease (de Jong et al. 2008; Power and Looi 2015), Parkinson's disease (Blesa, Trigo-Damas, and Obeso 2016; Wang et al. 2022), different forms of epilepsy (Natsume et al. 2003; Vetkas et al. 2022), schizophrenia (Buchsbaum et al. 1996; Byne et al. 2009), and obsessive-compulsive disorder (Van den Heuvel et al. 2016; Weeland et al. 2022).

Magnetic resonance imaging (MRI)-based structural and volumetric characterization of thalamic nuclei in humans has become increasingly important for both basic research and clinical purposes (Lozano 2000; Iglesias et al. 2018; Keun et al. 2021). Nevertheless, in vivo mapping of thalamic nuclei can present technical challenges since thalamic nuclear boundaries are notoriously difficult to visualize, for instance, even in standard T1-weighted (T1w) MRI (Magnotta et al. 2000; Iglesias et al. 2018; Najdenovska et al. 2019; Su et al. 2019; Rushmore et al. 2022). Another challenge can result from structural and volumetric biases induced by high levels of head motion during MRI (Reuter et al. 2015; Baum et al. 2018; Zacà et al. 2018), such as those occurring in patients with tremors, Alzheimer's diseases, and also healthy elderly adults (Van Dijk, Sabuncu, and Buckner 2012; Iglesias et al. 2017). While reducing scanning times can mitigate the probability of motion artifacts, it is also important to consider that undersampled techniques might be more sensitive to motion due to less data being collected. Therefore, in addition to reducing scan times to improve patient comfort, workflow, and throughput, adopting tools that allow for accurate segmentation of thalamic nuclei, even in the presence of small motion artifacts, can help address these challenges.

Compressed sensing (CS; Donoho 2006) is one among various acceleration techniques recently proposed for MRI. By only sampling a subset of the *k*-space rather than its full grid, CS allows for a faster acquisition of high-resolution MRI data (Lustig, Donoho, and Pauly 2007; Pauly 2008). CS has recently been applied to several T1w sequences, such as the standard vendor-provided magnetization-prepared rapid gradient echo (MPRAGE; Mugler III and Brookeman 1990) and its variant MP2RAGE (Marques et al. 2010). In general, reports are of comparable quality and volumetry to parent non-CS-accelerated sequences in a number of brain structures (Mair et al. 2019, 2020; Mönch et al. 2020; Mussard et al. 2020; Dieckmeyer et al. 2021; Ferraro et al. 2022), with biases at higher accelerations. So far, the effect of CS acceleration of various MPRAGE sequence variants has not yet been investigated on the volumetry of thalamic nuclei specifically. The acquisition of CS-accelerated structural images has the potential to help the structural and volumetric characterization of thalamic nuclei in patients with high level of head motion, especially since research protocols often combine multimodal MRI techniques that require long runtime scans.

The accurate segmentation of thalamic nuclei is another important factor for basic and clinical research. Together with faster scans, a reduction of data processing times without sensible effects on the outcome variables becomes an appreciated factor, especially when in vivo research employs large samples. Several brain segmentation tools have been proposed, among which FreeSurfer (Fischl et al. 2002; Fischl 2012) is well-known and commonly used (Despotović, Goossens, and Philips 2015). An alternative to FreeSurfer has recently been proposed, called FastSurfer (Henschel et al. 2020). FastSurfer is a deep learning-based and extensively validated whole-brain segmentation tool able to replicate FreeSurfer analyses in about 1 h, as opposed to FreeSurfer, which takes several hours. There is evidence indicating it as a robust alternative to FreeSurfer in cortical and subcortical structures (Henschel et al. 2020; Bloch and Friedrich 2021; Kemenczky et al. 2022; Müller et al. 2023) including the thalamus (Opfer et al. 2023). However, it remains unknown how the performance of FastSurfer for thalamic nuclei segmentation may be affected by T1w acceleration strategies.

In this study, we aimed to evaluate the robustness of thalamic nuclei volumetry by examining the effects of two key variables: the use of different MPRAGE acquisition variants with varying CS acceleration factors, and the application of thalamic nuclei segmentation methods with different processing speeds. Specifically, we assessed the robustness of thalamic nuclei segmentations initialized from either FastSurfer or FreeSurfer across several MPRAGE variants, including standard MPRAGE (5:32 min), multiecho MPRAGE (6:03 min), MP2RAGE (8:52 min), CS-MP2RAGE (3:40 min), and two CS-MPRAGE variants (2:04 min and 1:14 min).

2 | Materials and Methods

2.1 | Participants

In the present study, GeneRalized Autocalibrating Partial Parallel Acquisition (GRAPPA)-accelerated sequences (Griswold et al. 2002) are referred to as non-CS sequences. We used data from two samples: (i) Sample A with both non-CS and CS sequences: 15 healthy adults (mean age (SD) = 25.7 (3.5), range = [20.7, 32.5] years; 47% males) and (ii) Sample B with only non-CS sequences: 7 healthy adults (mean age (SD) = 30.2 (6.5), range = [24.1, 38.6] years; 57% males). No statistically significant

differences in age (Mann–Whitney U test: $U = 29$, $p > 0.10$) and gender ($\chi^2 = 0.11$, $p > 0.10$) of the two samples were detected with nonparametric analyses. Consequently, results for non-CS data are based on 22 subjects altogether, while CS results are based on 15.

2.2 | MRI Acquisition

Table 1 lists acquisition parameters of all the considered sequences. All subjects underwent 3T MRI (MAGNETOM Prisma, Siemens Healthcare, Erlangen, Germany) with a 64-channel head–neck radiofrequency receive coil. For each participant, the 3D T1w sequences were acquired in a single scanning session. Six 3D T1w sequences were acquired, all with 1 mm isotropic voxels, same spatial coverage, prescan normalize on, and no image filters: MP2RAGE (TR/TE = 5000/2.98 ms; TI = 700/2500; $\alpha = 4°/5°$; GRAPPA = 3; TA = 8:52 min), multiecho MPRAGE (meMPRAGE; TR = 2530 ms, $TE_{1–4} = 1.69/3.55/5.41/7.27$ ms, TI = 1100 ms, $\alpha = 7°$; GRAPPA = 2; TA = 6:03 min), "standard" MPRAGE (TR/TE/TI = 2310/3.48/1200 ms; $\alpha = 12°$; GRAPPA = 2; TA = 5:32 min; Mugler III and Brookeman 1990), research application CS-MP2RAGE (TR/TE = 5000/2.88 ms; $\alpha = 4°/5°$; samples/TR = 195; undersampling factor = 4.6; regularization factors = 0.0006/0.0004; TA = 3:40 min; Mussard et al. 2020), and two CS-MPRAGE (TR/TE/TI = 2300/2.88/900 ms; $\alpha = 9°$; samples/TR = 196; regularization factor = 0.0006; Mussard et al. 2020) with different acceleration factors: (i) undersampling factor = 3.6; TA = 2:04 min and (ii) undersampling factor = 6.6; TA = 1:14 min. More details on CS reconstructions can be found in Mussard et al. (2020). For the meMPRAGE image reconstruction, all echoes were averaged to yield one T1w image for the segmentations (Van der Kouwe et al. 2008). For the MP2RAGE reconstruction, a regularization was applied on the uniform image to remove typical noise in the background (O'Brien et al. 2014).

2.3 | Whole-Brain Segmentation

T1w images were processed through the novel FastSurfer (Henschel et al. 2020; https://deep-mi.org/research/fastsurfer) and the commonly used FreeSurfer (Fischl et al. 2002; Fischl 2012; https://surfer.nmr.mgh.harvard.edu) automated segmentation tools. The main distinctions between FastSurfer and FreeSurfer reflect their differences in computational steps: in contrast to FreeSurfer, which runs intensive computations like nonlinear atlas registrations, brain extraction, and intensity normalizations to achieve segmentations, FastSurfer utilizes convolutional neural networks (CNNs) to recognize and segment cortical and subcortical structures, subsequently using them for cortical surface reconstruction, labeling, and thickness parametrization. More details about the rationale and workflow of FastSurfer can be found in the original publication and its online companion (Henschel et al. 2020; https://deep-mi.org/research/fastsurfer).

With the segmentation method FastSurfer, T1w images were segmented using the *FastSurferCNN* pipeline, which runs whole-brain volumetric segmentations and yields equivalent data to the *aparc.DKTatlas + aseg.mgz* file of FreeSurfer, as well as via the *recon-surf* stream, which creates surface-based cortical thickness data from the *FastSurferCNN* segmentation.

With the segmentation method FreeSurfer (v. 7.1.1), T1w images were segmented through the *recon-all* stream, which performs all preprocessing steps, including motion and bias field corrections, as well as cortical and subcortical segmentations.

2.4 | Thalamic Nuclei Parcellation

Following whole-brain segmentations initialized from either FastSurfer or FreeSurfer, the thalamic nuclei were further

TABLE 1 | Outline of MRI sequence parameters for the 3D MPRAGE variants used.

	Sequence					
Parameter	**MP2RAGE**	**me MPRAGE**	**MPRAGE**	**CS-MP2RAGE**	**CS-MPRAGE**	
TA (min:sec)	8:52	6:03	5:32	3:40	2:04	1:14
Participant N	22	22	22	15	15	15
TR (ms)	5000	2530	2310	5000	2300	2300
TE (ms)	2.98	1.69/3.55/5.41/7.27	3.48	2.88	2.88	2.88
TI (ms)	700/2500	1100	1200	700/2500	900	900
Flip angle (deg)	4/5	7	12	4/5	9	9
Acceleration technique	GRAPPA	GRAPPA	GRAPPA	CS	CS	CS
Undersampling factor	3	2	2	4.6	3.6	6.6
Samples/TR	176	176	180	195	196	196
Regularization factor	*NA*	*NA*	*NA*	0.0006/0.0004	0.0006	0.0006
Voxel resolution (mm^3)	1	1	1	1	1	1

Note: From left to right, sequences are in descending order of acquisition time (TA, min:sec). Throughout the text, GRAPPA-accelerated sequences are referred to as non-CS-accelerated sequences. The two samples forming the dataset of this study did not differ in either age or gender (see Section 2 for details).
Abbreviations: CS, compressed sensing; NA, not applicable; TE, echo-time; TI, inversion time; TR, repetition time.

segmented separately using the thalamic parcellation tool developed by Iglesias et al. (2018; https://freesurfer.net/fswiki/ThalamicNuclei). This tool provides volumetric data for each thalamic nucleus, thus allowing us to evaluate the robustness of the results considering different initialization points from FastSurfer and FreeSurfer, for each MRI sequence.

To reduce the number of thalamic segmentation labels, we merged thalamic nuclei subdivisions as follows: pulvinar (PU; subdivisions: PuM, PuA, PuL, PuI), ventrolateral (VL; subdivisions: VLa, VLp), mediodorsal (MD; subdivisions: MDm, MDl), ventral anterior (VA; subdivisions: VA, VAmc); and intralaminar (IL; nuclei: CM, CeM, CL, Pc, Pf). The following are further thalamic nuclei considered in the present study for which we have not changed labels with respect to Iglesias et al. (2018): anteroventral (AV), laterodorsal (LD), lateral geniculate nucleus (LGN), lateral posterior (LP), limitans-suprageniculate (L-Sg), medial geniculate nucleus (MGN), medial ventral-reuniens (MVRe), paratenial (Pt), and ventromedial (VM). We relabeled nucleus VPL to VP by virtue of name consistency with other major thalamic nuclei (Jones 2007). Similar merging and relabeling schemes were used by other authors as well (e.g., Iglesias et al. 2018; Bocchetta et al. 2020; Tregidgo et al. 2023). The merged volume of a given thalamic nucleus was computed as the sum of its subdivisions' volumes, independently for each subject, sequence, segmentation tool, and hemisphere. For a complete description of nuclei colors and relabeling scheme, see Table S1.

2.5 | Dice Similarity Coefficients

We also used the dice similarity coefficient (DSC) to evaluate the 3D spatial similarity of thalamic nuclei segmentations related to the two main effects investigated in our study: (i) the within-sequence effects of segmentation initialization tool (FreeSurfer vs. FastSurfer) and (ii) the across-sequence effects when segmentations are initialized with FastSurfer, relative to the multiecho MPRAGE sequence used in the original thalamic segmentation study (Iglesias et al. 2018). The left- and right-hemispheric masks were merged for each subject, sequence, and segmentation initialization tool, independently for each thalamic structure using FSL. For the DSC analysis, the paratenial nucleus (Pt, mean volume across sequences = 7 mm^3) was excluded due to the absence of bilateral masks in more than 90% of data. For the remaining thalamic structures, the DSC was calculated independently for each subject and sequence. The DSC was computed as twice the ratio of the intersection of the segmentations to their union, with the formula present in Henschel et al. (2020). DSC computation was performed in Python (v. 3.10.13). DSC data visualization was performed with software R (v 4.2.2; R Core Team 2022).

2.6 | Statistical Analysis

Since we investigated within-subject volumetry across MPRAGE variants and did not compare individuals, we used raw thalamic nuclei volumes (mm^3) without adjusting for intracranial volume or thalamus size. Within-subject volumetric variability across sequences was evaluated using coefficients of variation (CV), defined as the ratio of the standard deviation of volumetric data across sequences to its mean, then averaging CV across subjects. CV computation was applied separately for the two segmentation tools considered in this study and for each thalamic structure. We assessed the similarity of volume variability in left- and right-hemispheric data using the modified signed-likelihood ratio test for equality of CV (Krishnamoorthy and Lee 2014), in both FastSurfer and FreeSurfer data, to see whether the dimensionality of the study variables could be reduced by averaging volumes across hemispheres.

To explore the relation between thalamic nuclei size and volume variation, we computed Pearson's correlation coefficient (r) between volumes and CV. Furthermore, to evaluate the consistency in volume variability for the two considered segmentation tools, we calculated Pearson's r between thalamic nuclei CV of FastSurfer- and FreeSurfer-initialized data.

Friedman rank-sum tests were used to assess sequence effects on volumetric data of thalamic structures. Friedman test is the nonparametric equivalent of a repeated-measure one-way analysis of variance (Friedman 1937). To investigate whether the proportion of sequence effects was different depending on the acceleration type (non-CS vs. CS accelerations), we used the paired samples McNemar's test on proportions with Yates' continuity correction for non-CS and CS data. Furthermore, we assessed sequence effect size using Kendall's W coefficients of agreement (Kendall 1948; Landis and Koch 1977). Kendall's W is the normalized Friedman test statistic, and it ranges between 0 (no agreement) and 1 (complete agreement).

We also evaluated the agreement between FastSurfer- and FreeSurfer-initialized thalamic nuclei volumes using Bland–Altman analysis (Bland and Altman 1986), and the intraclass correlation coefficient (ICC, Fisher 1936) as a measure of consistency between the two segmentation tools. ICC was computed considering all sequences together as well as separately. For each thalamic structure in the Bland–Altman analysis, normalized mean differences were computed as the absolute value of the ratio of the difference between volumes of the two tools to their mean.

As part of the quality assurance and in addition to the visual inspection of the segmentations, we calculated the signal-to-noise ratio (SNR) and the contrast-to-noise ratio (CNR) for each hemispheric thalamus segmented with FastSurfer. The mean signal and its standard deviation of left and right thalami were taken from FastSurfer's summary segmentation statistics (Henschel et al. 2020) and averaged across hemispheres. The SNR was defined as the ratio of the mean foreground signal to its standard deviation within the thalamus (Esteban et al. 2017; Yarach et al. 2021). We then computed group averages for each MPRAGE sequence variant. The CNR was computed as the absolute value of the difference between mean intensities in the thalamus and the white matter from the genu of the corpus callosum (gCC), divided by the standard deviation of the signal in the gCC (Okubo et al. 2016). For both SNR and CNR analyses, masks of hemispheric thalami and gCC were binarized with FSL from FastSurfer's file *aseg.mgz*, which provides segmentations of both the whole thalamus and corpus callosum subdivisions. Pairwise differences in sequences for both SNR and CNR measures were evaluated using Mann–Whitney U tests. U-values were converted to z-scores, and p-values adjusted for

multiple comparisons and compared to Bonferroni-corrected significance level $\alpha = 0.00625$.

Data visualization and statistical analyses were performed with software R (v 4.2.2; R Core Team 2022).

3 | Results

3.1 | T1-Weighted MRI Quality Assurance

Figure 1 shows T1-weighted images of a representative sample subject for qualitative comparison of MR images across MPRAGE variants. Image blurring increased expectedly with higher accelerations, though image contrast was well preserved across sequences.

Figure 2 shows a 3D rendering of thalamic nuclei (FreeSurfer-initialized data) in a representative sample subject, to highlight their anatomical localization within the thalamus. Figure 3 shows automated thalamic parcellations across sequences in a representative sample subject (FastSurfer). Visual inspection of the thalamic nuclei segmentations showed qualitative similarities for all MPRAGE variants, in segmentations initialized from both FastSurfer and FreeSurfer tools. This confirmed that the range of accelerations evaluated has sufficient quality for enabling automated subsequent thalamic nuclei segmentations from both segmentation tools. With this finding, we proceeded with a quantitative and systematic evaluation of how thalamic nuclei segmentation is affected by sequence and segmentation tools. Figure S1 shows automated thalamic parcellations across sequences in a representative sample subject for FreeSurfer-initialized data.

Figure S4 shows the group thalamus SNR and CNR distributions across the MPRAGE variants evaluated. Various thalamic SNR differences were observed across sequences. The highest SNR was given by meMPRAGE, while MP2RAGE had the lowest SNR values. Both meMPRAGE and MPRAGE showed higher SNR relative to MP2RAGE (both comparisons: $z = 5.68$; $p_{adj} < 0.00001$). Furthermore, within the CS-accelerated sequences, both versions of the CS-MPRAGE had higher SNR than CS-MP2RAGE ($z = 4.54$; $z = 4.38$; both $p_{adj} < 0.00001$). We also found SNR to be higher in CS-MP2RAGE than that in MP2RAGE ($z = 5.1$; $p_{adj} < 0.00001$). Finally, no difference in SNR was detected between the two versions of CS-MPRAGE with each other and between standard MPRAGE and the 1-min CS-MPRAGE.

With regard to thalamic CNR differences across sequences, we found that within the non-CS sequences, MP2RAGE had the highest CNR, both relative to meMPRAGE ($z = 5.35$, $p_{adj} < 0.00001$) and MPRAGE ($z = 5.68$, $p_{adj} < 0.00001$). Similarly, within the compressed sensing sequences, CS-MP2RAGE provided the highest CNR relative to the 2- and 1-min CS-MPRAGE ($z = 2.76$ and $z = 2.84$, respectively; both $p_{adj} < 0.01$). There were no significant CNR differences between these two CS-MPRAGE sequences. Finally, we found that the fastest sequence evaluated, namely the 1-min CS-MPRAGE, had higher CNR than its non-CS-accelerated parent sequence, the MPRAGE ($z = 3.06$; $p_{adj} < 0.01$).

3.2 | Within-Subject Sequence Effects

3.2.1 | Volume Variability Across Sequences

We evaluated the level of within-subject volumetric variability across MPRAGE variants in the two segmentation tools FreeSurfer and FastSurfer. Table 2 lists volumes and CV of thalamic nuclei across the various sequences (FastSurfer-initialized data). Figure 4 summarizes the within-subject volume variation in thalamic structures across MPRAGE variants. Group-averaged values of FastSurfer-initialized thalamic volumes are shown in descending order of volume size for all T1w sequences (Figure 4A). The within-subject volume variation across sequences, averaged across subjects, is shown for each thalamic structure for both FastSurfer (Figure 4B) and FreeSurfer (Figure 4C) segmentation initializations, grouped separately by CS and non-CS sequences. This shows how larger nuclei had similar, low variability (< 10%) regardless of acceleration, while smaller nuclei yielded lower variability with CS acceleration, particularly in FreeSurfer-initialized thalamic data (Figure 4C). Figure 4D shows that smaller nuclei were generally associated with higher volume variability across sequences, while Figure 4E shows that volume variability effects are consistent across the two segmentation initializations, FreeSurfer and FastSurfer.

3.2.1.1 | Whole Thalamus. FastSurfer-initialized data CV in the whole thalamus were 3.9% and 4.0% in the left and right hemispheres, respectively, while 4.5% and 3.9% in thalamic data initialized from FreeSurfer. We investigated potential hemispheric effects in thalamic volume variabilities for both segmentation initializations. The modified signed-likelihood ratio test for equality of CV did not reveal significant hemispheric differences in either of the two considered segmentation initializations. For this reason, we averaged thalamic volumes across hemispheres.

3.2.1.2 | Thalamic Nuclei. Considering FastSurfer-initialized data, 9 out of 15 nuclei showed CV lower than 10%, 4 out of 15 in the range of 10%–20%, and L-Sg was the nucleus with the highest volume variation across sequences (22.9%). Similarly, in FreeSurfer-initialized data, 10 out of 15 nuclei showed variability lower than 10%, four nuclei, namely MGN, LD, VM, and MV(Re), had variability in the range of 10%–20%, and the most variable nucleus across sequences was again L-Sg (36.6%). For this reason, L-Sg was excluded from further analyses.

As expected, we found volumetric variability across sequences to be inversely proportional to the volume of thalamic nuclei (Figure 4D). Averaging across hemispheres and sequences, and excluding whole thalamus and L-Sg data, we found significant negative correlations between CV and thalamic nuclei volumes in both FastSurfer- (Pearson's $r_{(12)} = -0.47$, $t = -1.84$, $p < 0.10$, 95% CI [−0.80, −0.08]) and FreeSurfer-initialized data (Pearson's $r_{(12)} = -0.49$, $t = -1.97$, $p < 0.10$, 95% CI [−0.81, −0.05]).

Furthermore, we found a strong association between CV of thalamic nuclei volumes from FastSurfer and FreeSurfer initializations (Figure 4E). Excluding whole thalamus and

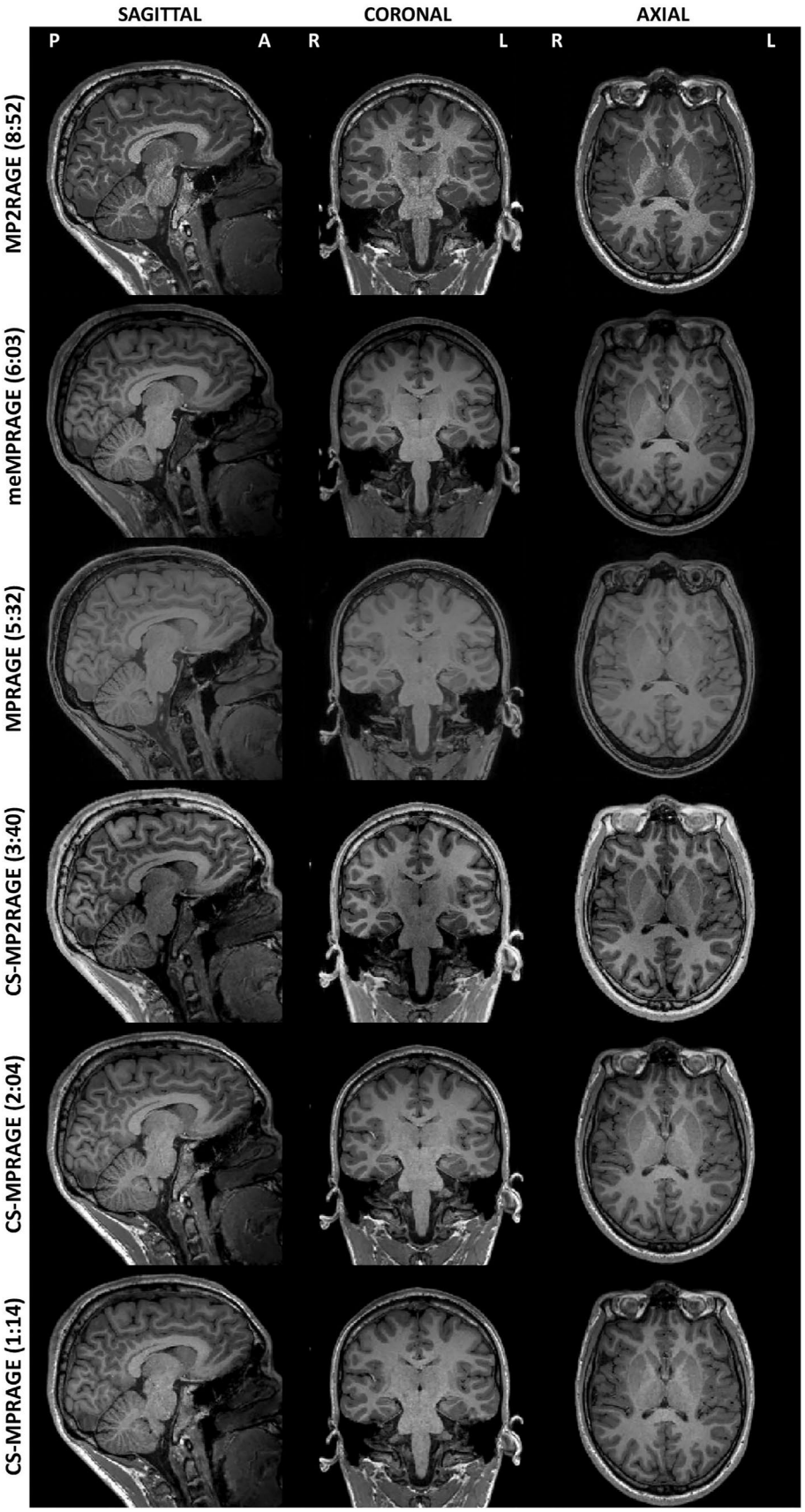

FIGURE 1 | T1-weighted image contrasts of differently accelerated MPRAGE variants. Qualitative comparisons of sagittal, coronal, and axial planes of a representative sample subject across the considered sequences (acquisition times in brackets are in minutes: seconds, sequences details in Table 1). Image brightness parameters were adjusted to better show tissue contrasts. Slices are taken at central thalamus (subject's native space). Sagittal images show the right hemisphere.

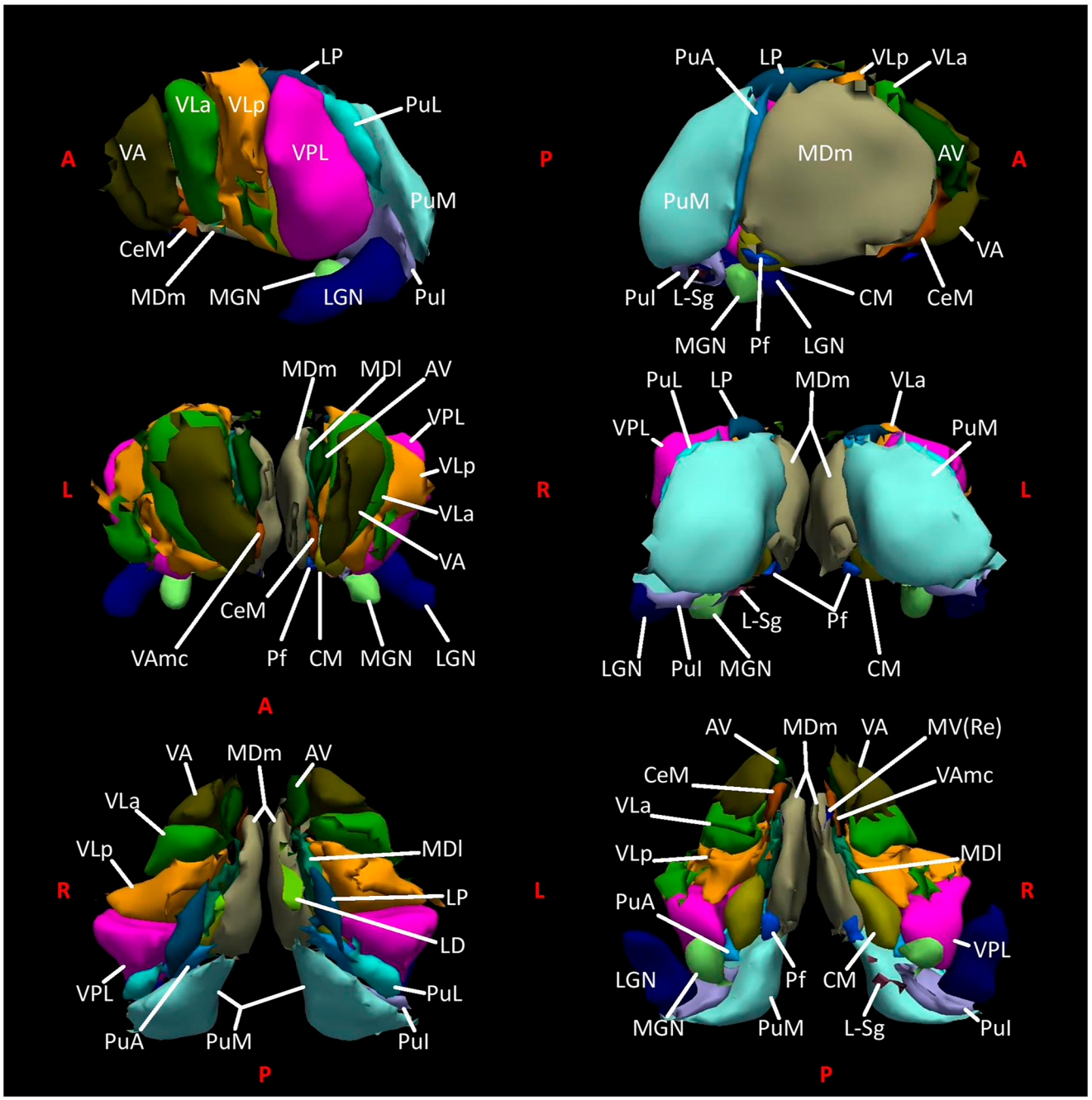

FIGURE 2 | Thalamic nuclei segmentation. FreeSurfer 3D rendering of thalamic nuclei in their lateral-medial (top row), rostral-caudal (middle row), and dorsal-ventral (bottom row) aspects on T1-weighted multiecho MPRAGE data of a representative sample subject. In the present study, thalamic nuclei subdivisions were merged as follows: PU (PuM, PuA, PuL, PuI); VL (VLa, VLp); MD (MDm, MDl); VA (VA, VAmc); and IL (CM, CeM, CL, Pc, Pf). See Table S1 for nuclei colors and details on the relabeling scheme.

L-Sg data, the linear fit was excellent (Pearson's $r_{(12)} = 0.93$, $t = 8.99$, $p < 0.00001$, 95% CI [0.80, 0.98]), showing consistency in thalamic volume variability for these two segmentation initializations.

3.2.2 | Sequence Effects and Effect Sizes

Figure 5 shows whole thalamus and thalamic nuclei volumes as initialized from FastSurfer segmentations for the considered MPRAGE variants. We investigated sequence effects in thalamic nuclei volumes across the various sequences, considering hemispheric data separately. Although Friedman tests yielded significant differences in nearly all thalamic structures, we observed no systematic bias in data according to sequence acceleration. In addition, a paired sample McNemar's test on proportions with Yates' continuity correction was performed to investigate marginal homogeneity of non-CS and CS data. Results revealed that the proportion of sequence effects was significantly higher in non-CS as compared to CS

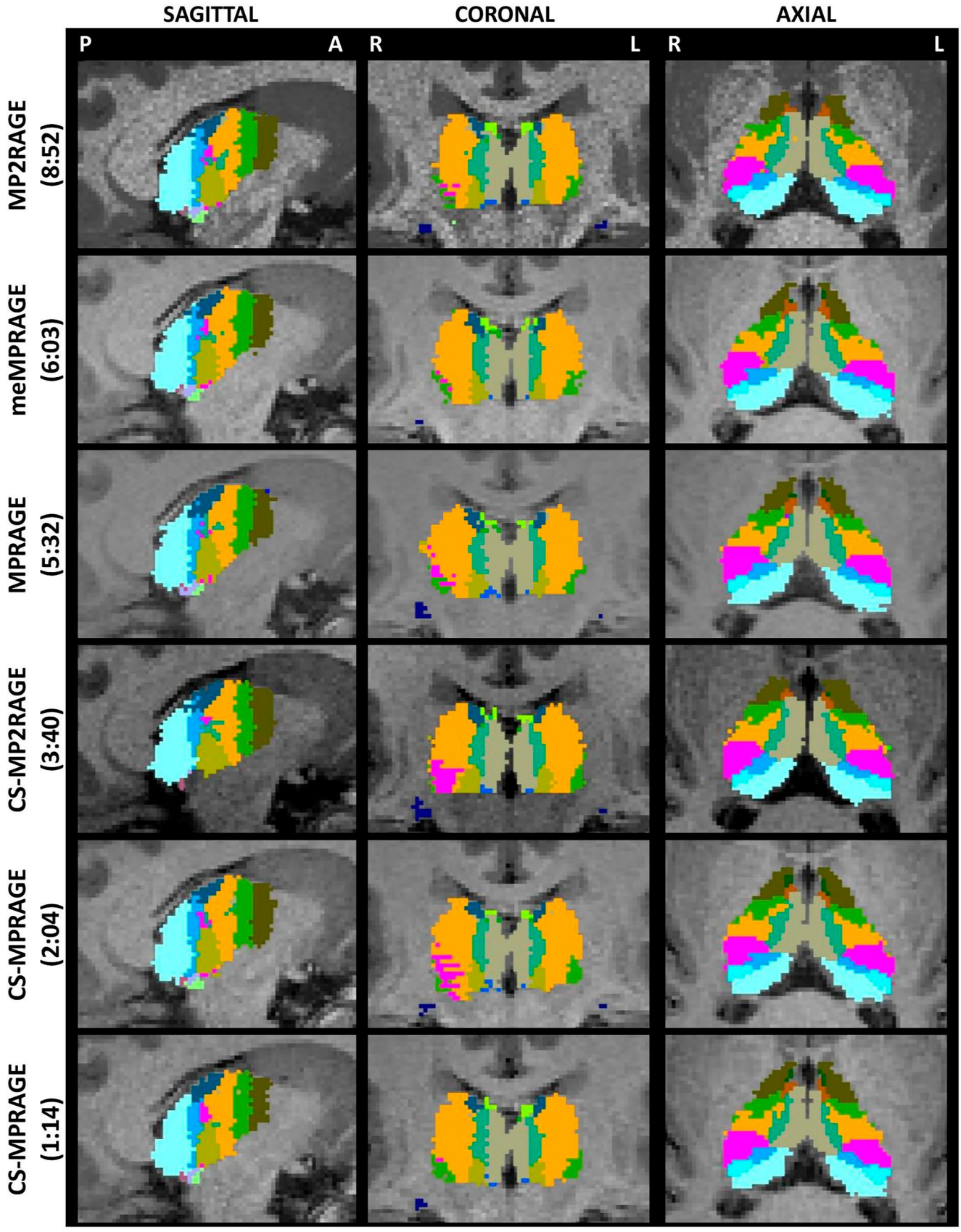

FIGURE 3 | Thalamic nuclei segmentations for differently accelerated MPRAGE variants. FastSurfer-initialized automated thalamic nuclei parcellations of a representative sample subject across the considered MPRAGE variants (acquisition times in brackets are in minutes:seconds, sequences details in Table 1). Sagittal, coronal, and axial planes of parcellations are with the same brightness parameters as in Figure 1. As in Figure 1, slices are taken at central thalamus (subject's native space). Sagittal images show the right hemisphere. Nuclei labels and colors as in Figure 2 and Table S1. FreeSurfer-initialized data of the same subject's native space can be seen in Figure S1.

TABLE 2 | Volumes, volume variability, sequence effects, and sequence effect sizes of thalamic structures across MPRAGE variants. FastSurfer-initialized volumetric segmentations for each MPRAGE sequence, group mean of within-subject coefficients of variation (CV) across MPRAGE variants, Friedman tests significance levels (adjusted *p*-values), and sequence effect sizes (Kendall's *W* coefficients) are presented for each thalamic structure.

		Volume (mm^3)								
						CS-MPRAGE				
Structure	Hemisphere	MP2RAGE (8:52)	meMPRAGE (6:03)	MPRAGE (5:32)	CS-MP2RAGE (3:40)	(2:04)	(1:14)	CV (%)	p_{adj} [a]	Effect size [b]
Thalamus	Left	6989 (1095)	6660 (707)	7162 (704)	7023 (892)	6929 (768)	6822 (812)	3.9	$<10^{-4}$	0.21
	Right	7017 (1169)	7015 (838)	7499 (834)	7006 (1114)	7330 (720)	7042 (716)	4	$<10^{-4}$	0.42
PU	Left	1895 (309)	1943 (260)	1763 (126)	1866 (161)	1931 (149)	1953 (203)	5.3	$<10^{-4}$	0.21
	Right	1858 (308)	1999 (227)	2144 (325)	1837 (203)	2077 (198)	2158 (215)	7.5	$<10^{-4}$	0.48
VL	Left	1412 (245)	1346 (184)	1548 (269)	1529 (229)	1415 (210)	1436 (236)	8	$<10^{-4}$	0.29
	Right	1459 (193)	1456 (228)	1539 (286)	1523 (246)	1446 (208)	1420 (170)	5.7	$<10^{-4}$	0.42
MD	Left	1179 (125)	1042 (115)	1023 (89)	1193 (153)	1053 (109)	1035 (66)	8.4	$<10^{-4}$	0.17
	Right	1199 (212)	1095 (105)	1070 (109)	1249 (229)	1095 (145)	1090 (182)	6.7	$<10^{-4}$	0.11
VP	Left	812 (150)	880 (147)	1029 (229)	894 (118)	897 (107)	898 (99)	10.7	$<10^{-4}$	0.29
	Right	817 (127)	946 (179)	1111 (237)	834 (124)	928 (119)	909 (168)	12.6	$<10^{-4}$	0.46
VA	Left	497 (86)	409 (47)	467 (54)	523 (92)	466 (54)	462 (68)	8.2	$<10^{-4}$	0.29
	Right	494 (84)	456 (63)	451 (46)	491 (66)	470 (63)	453 (38)	6.9	$<10^{-4}$	0.17
IL	Left	413 (66)	433 (63)	475 (76)	405 (39)	429 (51)	423 (52)	7.3	$<10^{-4}$	0.42
	Right	423 (68)	450 (77)	478 (79)	401 (50)	435 (46)	434 (45)	7.1	$<10^{-4}$	0.55
LGN	Left	304 (37)	264 (28)	248 (30)	272 (50)	288 (27)	283 (39)	9.4	$<10^{-4}$	0.25
	Right	275 (31)	262 (29)	264 (32)	254 (29)	281 (29)	274 (28)	5.2	<0.01	0.40
MGN	Left	147 (22)	124 (18)	134 (24)	90 (19)	132 (20)	132 (23)	14.5	$<10^{-4}$	0.44
	Right	166 (28)	143 (25)	133 (29)	107 (22)	150 (29)	141 (17)	13.7	$<10^{-4}$	0.46
AV	Left	135 (22)	114 (13)	130 (19)	138 (19)	130 (11)	126 (23)	9.9	$<10^{-4}$	0.15
	Right	144 (22)	139 (16)	139 (20)	139 (7)	141 (22)	137 (19)	6.2	*NS*	*NA* [d]
LP	Left	112 (24)	114 (24)	130 (25)	138 (22)	113 (19)	111 (29)	10.1	$<10^{-4}$	0.32
	Right	115 (30)	108 (16)	115 (26)	120 (13)	106 (9)	103 (22)	9	$<10^{-4}$	0.36

(Continues)

TABLE 2 | (Continued)

Structure	Hemisphere	Volume (mm^3) MP2RAGE (8:52)	meMPRAGE (6:03)	MPRAGE (5:32)	CS-MP2RAGE (3:40)	CS-MPRAGE (2:04)	CS-MPRAGE (1:14)	CV (%)	p_{adj} [a]	Effect size [b]
L-Sg	Left	45 (8)	34 (5)	34 (6)	16 (4)	33 (6)	34 (7)	23.6	*NA* [c]	*NA* [c]
	Right	40 (6)	35 (8)	37 (8)	15 (3)	33 (9)	35 (8)	22.3	*NA* [c]	*NA* [c]
LD	Left	32 (9)	22 (8)	29 (16)	29 (12)	23 (11)	25 (14)	19.7	$<10^{-4}$	0.29
	Right	36 (10)	25 (8)	23 (10)	25 (10)	24 (8)	26 (10)	21.1	$<10^{-4}$	0.38
VM	Left	18 (3)	23 (6)	29 (8)	22 (3)	22 (3)	22 (2)	18.7	$<10^{-4}$	0.42
	Right	19 (3)	27 (8)	31 (8)	20 (3)	22 (5)	24 (4)	19.8	$<10^{-4}$	0.46
MV(Re)	Left	18 (3)	13 (3)	15 (2)	16 (2)	16 (3)	16 (3)	12.4	$<10^{-4}$	0.25
	Right	19 (3)	16 (2)	16 (2)	17 (3)	18 (3)	17 (2)	11.9	$<10^{-4}$	0.25
Pt	Left	7 (1)	6 (1)	7 (1)	6 (1)	7 (1)	7 (1)	7.3	$<10^{-4}$	0.53
	Right	7 (1)	8 (1)	8 (1)	7 (1)	8 (1)	7 (1)	5.8	$<10^{-4}$	0.55

Notes: Median (interquartile range) volumes of the considered thalamic structures in the left and right hemispheres across MPRAGE variants (FastSurfer-initialized data). Coefficients of variation (CV) represent group-averaged within-subject volume variations across sequences. For each sequence, acquisition times (TA) are in brackets. From left to right, sequences are sorted in descending order of TA. From top to bottom, thalamic structures are sorted in descending order of mean volume across sequences. Thalamic nuclei labels as in Table S1.

Abbreviations: NA, not applicable; NS, nonsignificant.

[a] p-values refer to Friedman tests (Bonferroni-corrected $\alpha = 0.004167$).

[b] Effect sizes of sequence effects (Kendall's W coefficients); Interpretation: 0–0.4, small; 0.41–0.6, moderate; 0.61–0.8, substantial; 0.81–1, almost perfect (Landis and Koch 1977).

[c] Due to high volume variability, L-Sg was excluded from further analysis.

[d] Kendall's W for right LD was not computed following nonsignificant results of the Friedman test for this nucleus.

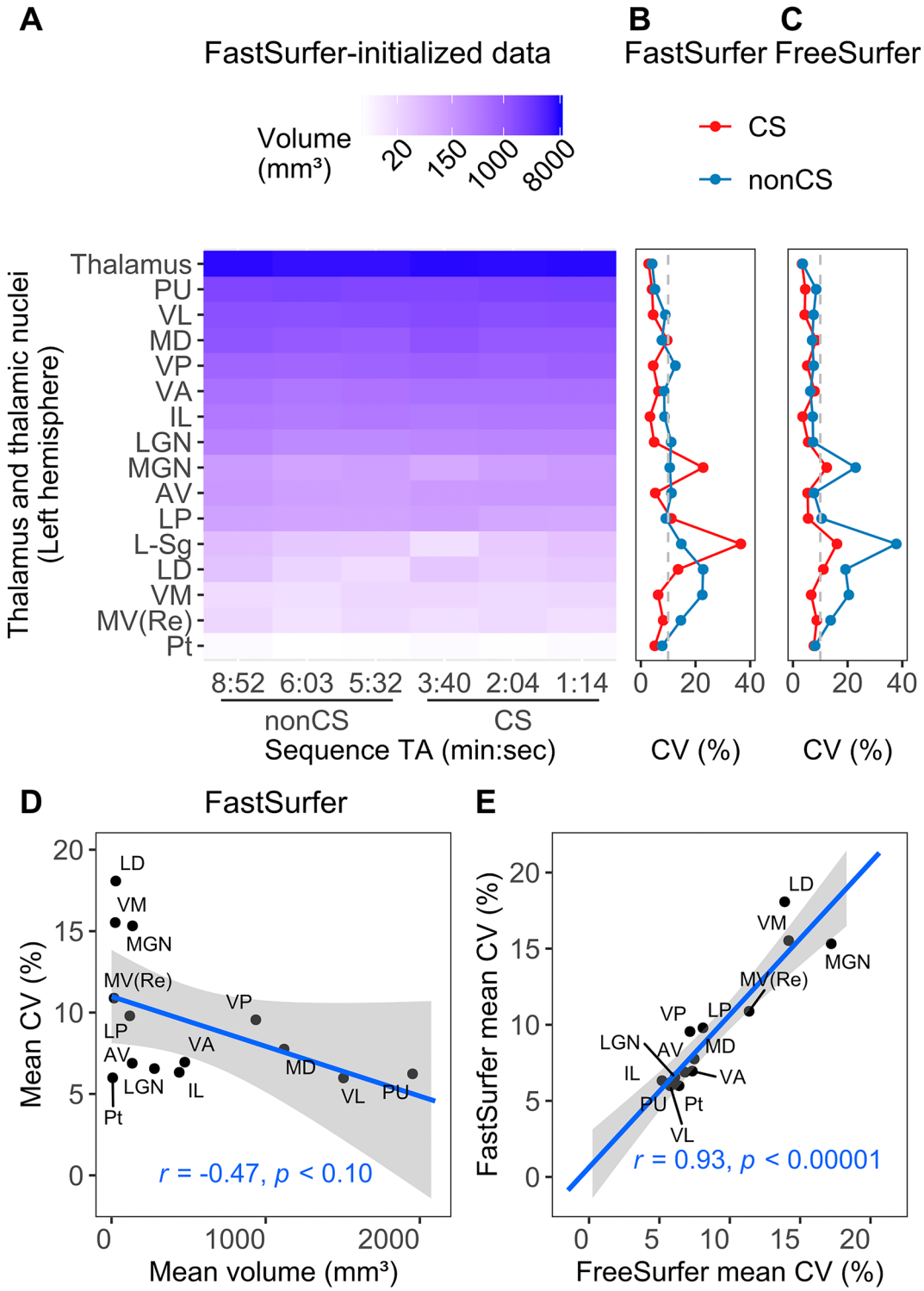

FIGURE 4 | Legend on next page.

data (80% vs. 33% of thalamic nuclei, respectively; $\chi^2_{(1)} = 10.56$, $p < 0.01$). Furthermore, we computed Kendall's W coefficients as a measure of sequence effect size. Effect sizes were small ($W < 0.40$) in 55% and moderate ($0.40 \leq W \leq 0.55$) in 45% of the considered thalamic structures. Table 2 lists volumes, Friedman test significances, and Kendall's W coefficients in the considered thalamic structures and sequences (FastSurfer-initialized data).

3.3 | Volume Correlations

To evaluate sequence biases in thalamic segmentations, we computed pairwise Pearson's r coefficients for all MPRAGE sequence combinations (FastSurfer-initialized data). All correlations were positive, ranging between 0.25 and 0.97. Figure 6 presents correlation matrices for pairs of sequences in the considered thalamic structures (FastSurfer intializations).

3.3.1 | Whole Thalamus

In the whole thalamus, we observed excellent volumetric correlations for all pairs of sequences (Pearson's r range = [0.73, 0.97]). The lowest value of r was observed between MPRAGE and CS-MP2RAGE volumes, while the highest was between MP2RAGE and CS-MP2RAGE volumes.

3.3.2 | Thalamic Nuclei

In 10 of 14 thalamic nuclei we found strong correlations regardless of sequence pair (Pearson's r range = [0.45, 0.96]). Moderate correlations were found in the MD nucleus only between standard MPRAGE and CS-MP2RAGE volumes ($r = 0.32$), as well as in LGN between MP2RAGE and MPRAGE volumes ($r = 0.44$). Furthermore, the weakest correlations were almost exclusively involving standard MPRAGE and were observed in the small nucleus MV(Re) between MPRAGE and CS-MP2RAGE volumes ($r = 0.25$), as well as in the major nucleus PU between MPRAGE and MP2RAGE ($r = 0.29$).

3.4 | FastSurfer and FreeSurfer Initializations: Thalamic Nuclei Segmentation Robustness

In the present study, we also assessed the robustness of the thalamic nuclei parcellation according to the two segmentation tools FastSurfer and FreeSurfer used as initializations. Overall, we observed good qualitative agreement between the two tools, despite slight differences mainly in lateroventral territories of the thalamus in the majority of participants. Figure 7 shows the results of the Bland–Altman analysis comparing thalamic nuclei volumetric data as segmented from the two tools. Relevant normalized volume differences were observed only in the small nuclei MGN and LD, the highest differences being on standard MPRAGE data for both nuclei.

Considering all sequences together, ICC between FastSurfer- and FreeSurfer-initialized thalamic volumes was 0.998 (95% CI [0.998, 0.999]). In individual sequences, ICC ranged between 0.996 and 1, the lowest value being with CS-MP2RAGE data and the highest with MP2RAGE.

3.5 | Spatial Similarity of Thalamic Nuclei: Effects of Segmentation Initialization and T1w Sequence

Figure 8A shows the within-sequence spatial segmentation similarity between FastSurfer and FreeSurfer initializations, for each thalamic structure in the various sequences. High spatial agreement was found for the whole thalamus (mean DSC = 0.9, range = [0.75, 0.95]) and in the major thalamic nuclei (those larger than 400 mm^3: PU, VL, MD, VPL, VA, and IL; DSC range = [0.78, 0.92]), considering all T1w sequences. The lowest mean DSC were observed in small nuclei VM and MV(Re).

Figure 8B shows across-sequence spatial segmentation similarity of thalamic structures initialized by FastSurfer (within-subject comparisons of each sequence relative to meMPRAGE). High spatial agreement was found for the whole thalamus (mean DSC = 0.89, DSC range = [0.71, 0.96]) and in the major nuclei (DSC range = [0.64, 0.82]). The lowest mean DSC were observed in small nuclei LD and MV(Re), and particularly in nucleus VM.

4 | Discussion

In the present study, we found that T1-weighted MPRAGE variants, from about 9 to 1 min acquisition times and accelerated with the CS technique, provide human brain images with adequate quality to enable automated segmentation of subcortical thalamic nuclei at 3T. In particular, we show that, despite some degree of within-subject variation across sequences, higher accelerations are able to provide thalamic volumetric data of comparable magnitude to standard MPRAGE variants. In addition to this, we found high correlations of thalamic nuclei volumes across sequences, despite some lower correlations particularly in smaller nuclei and with data from the standard MPRAGE sequence. Furthermore, we found that the novel segmentation tool FastSurfer can be a faster whole-brain segmentation method alternative to its counterpart FreeSurfer, which can be used as a starting point in the subsequent volumetric analysis of thalamic nuclei.

4.1 | T1-Weighted MRI Quality Assurance

A quality assurance of the considered MPRAGE variants revealed adequate quality of brain MR images. As expected,

FIGURE 4 | Within-subject volume variation in thalamic structures across MPRAGE variants. (A) Thalamic volumes (logarithmic color-coding by size, FastSurfer-initialized thalamic data) for each MPRAGE variant, grouped as noncompressed sensing (non-CS) and compressed sensing (CS) accelerations, and listed by decreasing acquisition times (TA: 8:52, MP2RAGE; 6:03, meMPRAGE; 5:32, MPRAGE; 3:40, CS-MP2RAGE; 2:04 and 1:14, CS-MPRAGE; TA is in minutes:seconds). Left hemispheric data were presented; right-hemispheric data were similar; (B) Within-subject coefficients of variation (CV) across MPRAGE sequences for thalamic structures (left and right hemispheres averaged), considering CV from non-CS (blue) and CS (red) sequences separately in FastSurfer-initialized thalamic nuclei segmentations. (C) Same as in panel (B), but using FreeSurfer-initialized thalamic nuclei segmentations; (D) Negative correlation trend between thalamic nuclei CV and volume (FastSurfer-initialized thalamic data averaged across hemispheres, sequences, and segmentation initializations). (E) Significant positive correlation between CV of FreeSurfer- and FastSurfer-initialized thalamic segmentations (data averaged across hemispheres and sequences). In panels (B) and (C), the gray dashed line represents a CV of 10% for visual reference purposes; thalamic labels correspond to the list on the left-hand side of panel (A). In panels (D) and (E), whole thalamus and L-Sg nucleus were excluded (see text for details); including whole thalamus data in the linear fit did not alter results significantly for both associations (results not reported); Pearson's r coefficients and their significance are presented; regression models show 95% confidence intervals of predictive values. In all panels, FastSurfer and FreeSurfer labels refer to the two segmentation initializations. Thalamic nuclei labels in Table S1. FreeSurfer-initialized thalamic volumes are shown in Figure S2.

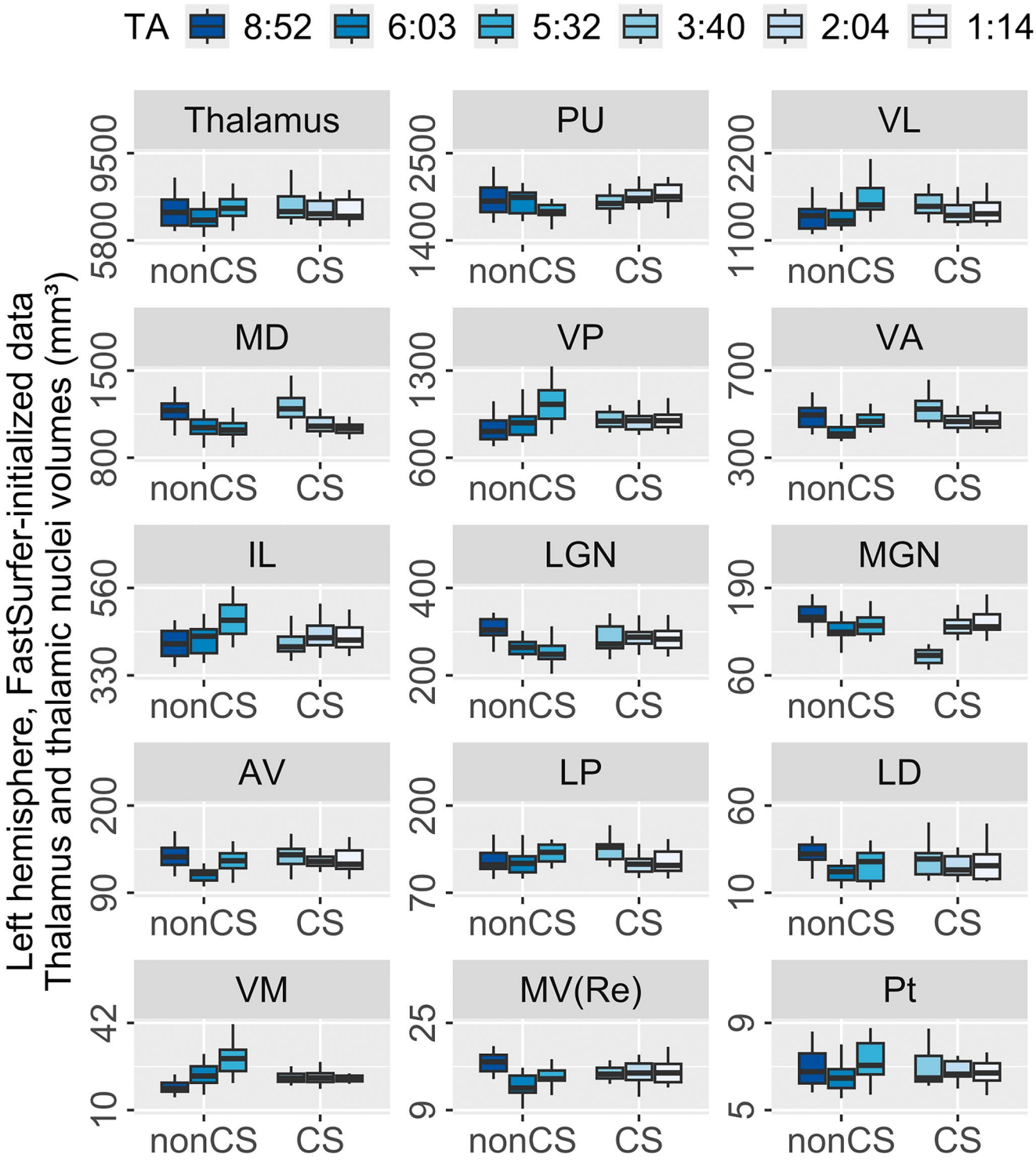

FIGURE 5 | MPRAGE sequence effects on thalamic volumes. FastSurfer-initialized volumetric segmentations in thalamic structures (group median and interquartile range, left hemisphere) for each MPRAGE sequence (see Table 1 for details on sequences). For each structure, box-and-whiskers are color-coded, sorted in descending order of acquisition time (TA), and grouped as noncompressed sensing (non-CS) and compressed sensing (CS)-accelerated sequences; Friedman tests yielded significant sequence effects for all thalamic structures in the left hemisphere (see Table 2). Right hemisphere was similar. Sequence TA (min:sec): 8:52, MP2RAGE; 6:03, meMPRAGE; 5:32, MPRAGE; 3:40, CS-MP2RAGE; 2:04 and 1:14, CS-MPRAGE. Thalamic nuclei labels as in Table S1. FreeSurfer-initialized thalamic volumes are shown in Figure S2.

this result is in agreement with previous evidence covering the cortex and subcortical regions, including the whole thalamus (Mair et al. 2019, 2020; Mussard et al. 2020; Dieckmeyer et al. 2021). To the best of our knowledge, there is currently a lack of evidence concerning volume variations as a function of CS accelerations of MPRAGE sequences in thalamic nuclei specifically. Hence, the present study fills this gap showing that good image quality can be achieved with CS accelerations also in structures as relatively small as thalamic nuclei, whose borders can be particularly elusive to 3T structural MRI contrasts

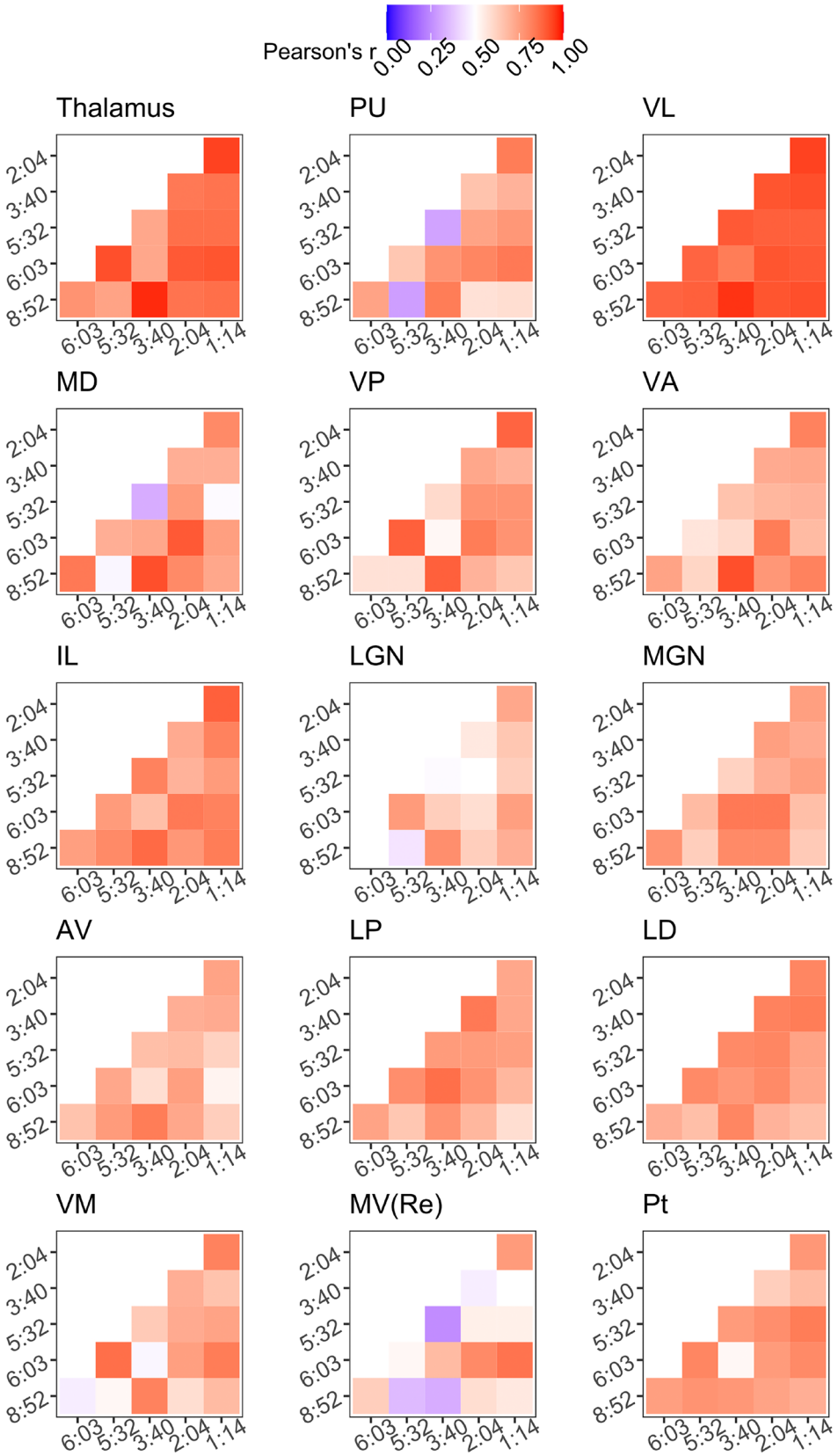

FIGURE 6 | Pairwise correlations of thalamic volumes across MPRAGE variants. Thalamic volume correlations for pairs of sequences are presented as color-coded Pearson's correlation coefficients (r, FastSurfer-initialized data). For each correlation matrix, sequence acquisition times (min:sec) are displayed on the axes (8:52, MP2RAGE; 6:03, meMPRAGE; 5:32, MPRAGE; 3:40, CS-MP2RAGE; 2:04 and 1:14, CS-MPRAGE). Pearson's r interval, shown in legend, ranges from 0 to 1. Thalamic nuclei labels as in Table S1. Pairwise correlations in FreeSurfer-initialized thalamic data are presented in Figure S3.

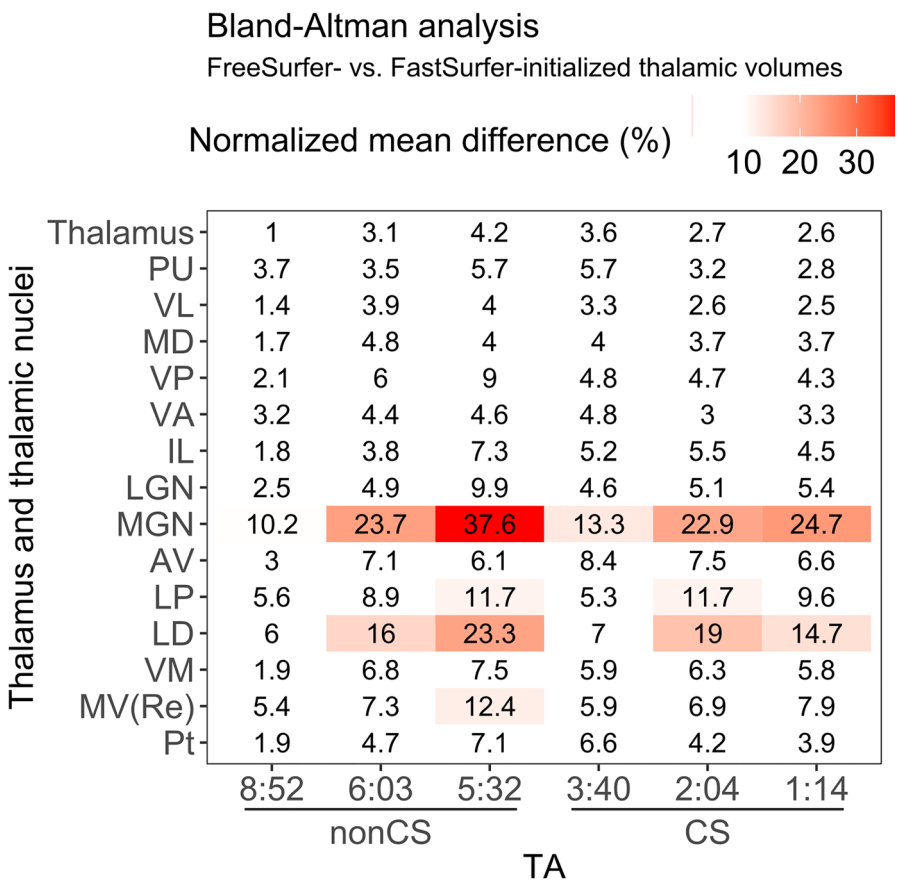

FIGURE 7 | Within-subject and within-sequence comparison of FreeSurfer- and FastSurfer-initialized thalamic segmentation across MPRAGE variants. Bland–Altman analysis comparing thalamic volumes from the two considered segmentation tools. For each thalamic structure, normalized mean differences were computed as the ratio of the absolute difference between volumes of the two tools to their mean, for each subject and then group averaged. Here, normalized mean differences are reported as the mean across subjects, expressed as percentage, and color-coded. Only volume variabilities higher than 10% were colored, to better highlight the highest differences (notably, nuclei MGN and LD, mean volumes across sequences of 126 and 30 mm^3, respectively). On the *x*-axis, sequences are sorted in descending order of acquisition time (TA, min:sec), and grouped as noncompressed sensing (non-CS) and compressed sensing (CS); on the *y*-axis, thalamic structures are sorted in descending order of mean volume across sequences. Thalamic nuclei labels as in Table S1.

and parcellation techniques (Magnotta et al. 2000; Iglesias et al. 2018; Najdenovska et al. 2019; Su et al. 2019; Rushmore et al. 2022).

As far as segmentation quality and volumetry of thalamic nuclei are concerned, we found good correspondence with the literature (Benedict et al. 2013; Schoonheim et al. 2015; Iglesias et al. 2018; Shin, Lee, and Park 2019). We observed some degree of variability in segmentation quality, particularly in standard MPRAGE data. It is known that the standard MPRAGE sequence performs suboptimally when separating cerebral tissues with not only T1 but also T_2* and proton density differences (Marques et al. 2010; Mussard et al. 2020) and provides insufficient contrast to delineate thalamic nuclei specifically (Sudhyadhom et al. 2009; Tourdias et al. 2014; Tohidi et al. 2023). We hypothesize that the volumetric variability we observed on standard MPRAGE data relates to its suboptimal contrast at gray–white matter interfaces particularly, a factor that could have driven the segmentation algorithm toward a misclassification of voxels, labeling, for instance, voxels of the internal capsule as belonging to the thalamic gray matter. With respect to other contrasts, this voxel misclassification on standard MPRAGE data specifically could have produced differences mainly along lateral thalamic boundaries, overshooting voxel labels into white matter territory. This explanation is also in line with what has been stated by the developers of the thalamic parcellation tool we employed (Iglesias et al. 2018). Furthermore, these observations are consistent with the lower correlations we found in this study between standard MPRAGE data and the other sequences, for example, in voluminous nuclei such as LGN, PU, and VP, all rich in fibers or placed directly at gray–white matter interfaces (Grieve, Acuña, and Cudeiro 2000; Fujita et al. 2001; Jones 2007; Iglesias et al. 2018). As far as other MPRAGE variants are concerned, segmentations proved to be robust and of comparable quality among CS-accelerated sequences, as did standard MP2RAGE and meMPRAGE data.

As part of our quality assurance, we evaluated the SNR in the thalamus across various accelerated MPRAGE sequences. We found that meMPRAGE provided the highest SNR, with no significant differences between standard MPRAGE (5 min 32 s) and the fastest CS-MPRAGE (1 min 14 s). These findings align with previous studies indicating that the regularization factor in CS

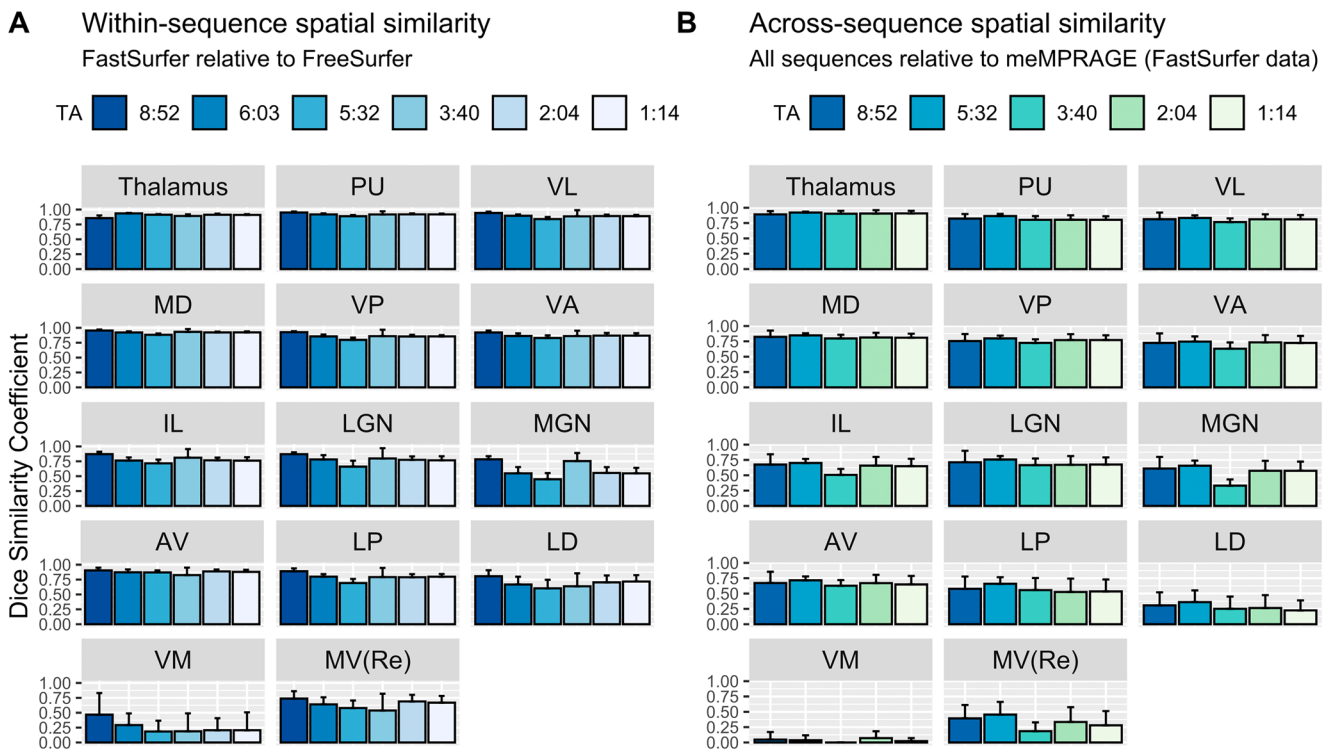

FIGURE 8 | Spatial similarity of thalamic nuclei segmentations using Dice Similarity Coefficient (DSC) analysis. (A) DSC in the whole thalamus and thalamic nuclei comparing FreeSurfer- vs. FastSurfer-initialized thalamic nuclei segmentations in MPRAGE variants. (B) DSC in the whole thalamus and thalamic nuclei comparing all sequences relative to multiecho MPRAGE (meMPRAGE) in FastSurfer-initialized thalamic data. In both panels, error bars represent one standard deviation from mean DSC across subjects. Thalamic structures are sorted in descending order of mean volume across sequences. For each structure, sequences are color-coded and sorted in descending order of acquisition time (TA). Thalamic nuclei labels in Table S1. Sequences TA (min:sec): 8:52, MP2RAGE; 6:03, meMPRAGE; 5:32, MPRAGE; 3:40, CS-MP2RAGE; 2:04 and 1:14, CS-MPRAGE.

sequences can maintain or even enhance SNR at high acceleration factors (Mair et al. 2019, 2020). Given that these sequences are typically optimized for CNR for segmentation purposes, we also examined thalamic CNR effects. Our results confirmed the CNR advantages of MP2RAGE over other MPRAGE variants when using noncompressed sensing acceleration (Marques et al. 2010; Okubo et al. 2016; Trotier et al. 2022). Additionally, we verified that despite their acquisition time difference, MP2RAGE (8 min 52 s) and CS-MP2RAGE (3 min 40 s) have comparable CNR in the thalamus. Our findings extend previous research by showing that CS-MP2RAGE has higher CNR than faster CS-MPRAGE variants, and that the fastest CS-MPRAGE (1 min 14 s) provides significantly higher CNR than standard MPRAGE (5 min 32 s).

Altogether, these quality assurance results suggest that the volumetry of thalamic nuclei can be investigated effectively also with CS-accelerated MPRAGE variants at acquisition times of about 1–2 min, as valid substitutes to longer and more conventional MPRAGE sequences.

4.2 | Within-Subject Sequence Effects

We found that the choice of MPRAGE variants introduces variability in the volumes of thalamic nuclei. More specifically, CV (FreeSurfer data) were above 10% in a third of the considered thalamic structures, consisting of smaller nuclei.

It is known that smaller brain structures, such as hippocampus and amygdala, which like the thalamus have a predominant composition of gray–white matter interfaces, exhibit high volume variabilities in volumetric studies (Bartzokis et al. 1993; Pruessner et al. 2000; Mueller et al. 2007), particularly when MR images differ in acquisition methods (Seiger et al. 2021). We hypothesize that the volume variations we observed in thalamic nuclei are related to their size, rather than being driven by CS accelerations. Indeed, the fact that we observed volume variations of less than 10% in bigger nuclei and less than 5% in the whole thalamus suggests that variations could relate to the size of nuclei, a result further supported by the negative correlation we found between CV and mean volumes of thalamic nuclei.

We also performed a volumetric analysis considering non-CS and CS data separately. We observed lower volume variations with CS data generally, notably in smaller thalamic nuclei as well. We also found a higher proportion of significant sequence effects in non-CS data as compared with CS data. Altogether, these results suggest higher volume variabilities particularly in non-CS data and small thalamic nuclei. We speculate that these results are due to the different MPRAGE variants used in this study. The non-CS sequences, namely MPRAGE, meMPRAGE, and MP2RAGE, are quite heterogeneous in terms of acquisition methods: MPRAGE is composed of only one single-echo T1-weighted image (Mugler III and Brookeman 1990), meMPRAGE results from averaging

four different echoes (Van der Kouwe et al. 2008), and the MP2RAGE uniform image is produced with a particular combination of volumes that rules out B_1 contributions to the image, using a single-echo approach (Marques et al. 2010). On the other hand, a comparison of thalamic nuclei volumetry across the CS sequences in this study, namely CS-MP2RAGE and the two versions of CS-MPRAGE, are all single-echo and differ mostly in the *k*-space undersampling factor which shortens acquisition times. Even if some degree of variability in the acquisition methods is preserved across the CS group as well, since the CS-MP2RAGE acquisition method differs from CS-MPRAGE, the fact that two out of three sequences in the CS group are almost identical could have driven the lower volume variability that we observed here, in contrast to the non-CS group, more heterogeneous in terms of acquisition protocols.

In addition to this, we found significant sequence effects for all the considered thalamic nuclei. However significant the volume variability across MPRAGE variants may be in our study, the effect sizes of sequence effects were small (Kendall's $W \leq 0.4$) in the majority of the considered thalamic structures, with the rest of the nuclei yielding moderate effects (W range = [0.41, 0.55]). This result indicates that sequence effects might play a little role in the observed volume variability altogether. In fact, it further suggests that the volume variability could ensue from a combination of acquisition methods, particularly in relation to non-CS sequences, and anatomical characteristics of thalamic nuclei, their size, and white matter fraction possibly being the most prominent factors.

In the light of this, the volume variability in thalamic nuclei that we observed could potentially be attributed to the combined effects of nuclei sizes and choice of CS acceleration. Nonetheless, the fact that the whole thalamus and major thalamic nuclei were less variable than minor nuclei, and that the observed sequence effects were little meaningful, suggests that the use of CS-accelerated MPRAGE sequences can be an effective approach in the volumetric characterization of thalamic nuclei.

4.3 | Volume Correlations

We also evaluated volume correlations across pairs of MPRAGE variants in the considered thalamic structures (FastSurfer segmentation initializations). The strongest correlations were seen in the whole thalamus, major nuclei VL, VP, VA, and IL, as well as in minor nuclei MGN, LP, LD, and Pt across all pairs of sequences. It is interesting to note that weak correlations were observed in the major nuclei PU and MD when standard MPRAGE data was considered. Weak correlations were also observed in the minor nucleus MV(Re) involving standard MPRAGE data in 2 out of 3 weak correlations. Tagen together, these results further suggest that standard MPRAGE sequence might not be the first-choice approach when characterizing thalamic nuclei structurally with MRI.

As previously mentioned, standard MPRAGE is known to perform suboptimally when separating tissues with different properties in certain brain regions (Marques et al. 2010; Mussard et al. 2020). Our correlational results, specifically in nuclei VP, PU, MD, and LGN when standard MPRAGE data were involved, suggest that the lower contrast that this sequence provides, for instance, in portions of the thalamus interfacing white matter structures (e.g., internal capsule, thalamic radiations, and internal medullary lamina), could bias the segmentation of these nuclei, hence subsequent volume correlations. Alonso et al. (2021) and Ferraro et al. (2022) found evidence that the volume of the whole thalamus can change significantly in relation to the choice of MPRAGE variants. These authors included standard MPRAGE in their comparisons with a single other CS-accelerated MPRAGE variant, and did not investigate sequence effects in thalamic nuclei exclusively, by reason of their main interest in other cortical and subcortical structures. In the light of all this, the choice of standard MPRAGE sequence as the only comparison term with CS-accelerated ancillary sequences might not be optimal for analyses in the thalamus area. Our data suggest that other sequence variants could be considered or included to fully appreciate potential differences across sequences, especially in studies including thalamus and/or thalamic nuclei.

High correlations on all the considered thalamic structures were observed between the two CS-accelerated MPRAGE sequences. As previously mentioned, they have an almost identical acquisition method, their only difference being *k*-space sampling factor. This characteristic could explain the high correlation values across thalamic nuclei observed between these two CS-accelerated MPRAGE sequences.

The low correlations we observed in the PU nucleus were a puzzling result. Since it is one of the most voluminous nuclei in the primate thalamus (Grieve, Acuña, and Cudeiro 2000; Ferris et al. 2013), we expected its volume to be less variable across sequences. On the contrary, it yielded two of the lowest correlations of the dataset. In this regard, we hypothesize that the grouping procedure we used to merge the PU subdivisions into a single entity could be at the basis of the observed low correlations in this nucleus specifically. By performing separate analyses of the four subdivisions of PU, we found that the subdivisions PuM, PuA, and PuI, but not PuL, had weak correlations involving standard MPRAGE data, with correlations going slightly below zero in the subdivision PuA between standard MPRAGE and MP2RAGE, and standard MPRAGE and CS-MP2RAGE (data not shown). This finding could relate partly to the aforementioned limitation of standard MPRAGE when segmenting different tissues, especially when compared, for instance, to the excellent contrast provided by MP2RAGE sequences. Furthermore, given the high range of cortico-pulvino-cortical connections subserving a wide variety of cognitive functions (Sherman and Guillery 2006; Fiebelkorn and Kastner 2020), we speculate that a differential proportion of white matter fibers could innervate the four subdivisions of the PU nucleus. By virtue of the poorer contrast of standard MPRAGE data with respect to other sequence contrasts, the differential proportion of white matter fibers in nucleus PU could ultimately have yielded weaker correlations when standard MPRAGE data were involved.

4.4 | FastSurfer and FreeSurfer Initializations: Thalamic Nuclei Segmentation Robustness

To the best of our knowledge, we provide first evidence that thalamic parcellations (Iglesias et al. 2018) can be obtained from FastSurfer segmentation initializations (Henschel et al. 2020) as well, in addition to segmentations using the FreeSurfer software, as mentioned by the authors of the thalamic nuclei parcellation tool in their guidelines (Iglesias et al. 2018). We assessed the robustness of the thalamic nuclei segmentation tool to the initializations from FastSurfer or FreeSurfer, and observed overall good qualitative agreement for both initializations. Bland–Altman analysis revealed notable differences only in the small nuclei MGN and LD, the highest differences being on standard MPRAGE data, while excellent ICC suggests a very high consistency between the two segmentation tools for all sequences.

FastSurfer has been recently proposed as an alternative to the intensive-runtime FreeSurfer whole-brain segmentation tool, providing comparable volumetric results to its counterpart in a number of brain regions (Henschel et al. 2020; Bloch and Friedrich 2021; Kemenczky et al. 2022; Müller et al. 2023), including the whole thalamus (Opfer et al. 2023). Our findings are in line with the literature and extend their validity to the thalamic nuclei specifically.

Taken together, our findings suggest that the characterization of thalamic nuclei with 3 T MRI in humans could benefit from both the use of CS accelerations and the segmentation initializations provided by the FastSurfer tool, whose combined effect can optimize the schedules required in multiple steps of MRI volumetric studies in terms of time consumption.

Furthermore, by showing the feasibility of structural and volumetric analysis with MRI data taken at short acquisition times, our findings pave the way to future studies aiming to characterize thalamic nuclei structural, diffusional, connectional, and functional profiles in either healthy subjects or highly kinetic populations, such as, for instance, elderly people and patients (Van Dijk, Sabuncu, and Buckner 2012; Iglesias et al. 2017; Madan 2018; Noor et al. 2020).

4.5 | Spatial Agreement of Larger Thalamic Nuclei Segmentations

We assessed the spatial similarity of thalamic nuclei segmentations using the DSC. We found good agreement between FreeSurfer- and FastSurfer-initialized thalamic data within T1w sequences, with DSC values ranging from 0.78 to 0.95 for the whole thalamus and major thalamic nuclei. Our results are in good agreement with the few studies that have specifically reported DSC values for FastSurfer segmentations of the whole thalamus specifically. In their work introducing FastSurfer, Henschel et al. (2020) performed Dice analyses comparing FastSurfer to FreeSurfer segmentations across 33 different subcortical structures using MPRAGE data from several public datasets (e.g., ADNI, HCP, OASIS1; see Henschel et al. 2020 for details). They reported DSC values ranging from 0.87 to 0.9 for subcortical structures across the various datasets. In another study, Opfer et al. (2023) proposed a novel whole-thalamus segmentation method consisting of a 3D CNN trained on adult human brain data from 170 MRI scanners at 1.5 and 3 T, collecting data from several databases. These authors reported a DSC of 0.86 for both their proposed segmentation method and for FastSurfer whole-thalamus segmentations relative to manual segmentations, but did not include FreeSurfer automated segmentation of this subcortical structure in their analyses. In another work, Ferraro et al. (2022) obtained DSC values of 0.86 and 0.88 in the left and right thalamus, respectively, comparing FreeSurfer segmentations on conventional MPRAGE and CS-MP2RAGE data. Our study extends these previous works by providing new evidence of high spatial similarity between FreeSurfer and FastSurfer not only in the thalamus as a unitary structure but also in its major subdivisions. This result suggests that FastSurfer data can be used effectively and alternatively to FreeSurfer as a starting point from which to segment thalamic nuclei, with the advantage of reducing individual subject data processing times by several hours each.

We also explored the variability of FastSurfer-initialized segmentations across different MPRAGE variants relative to the multiecho MPRAGE sequence. Despite a slight reduction in spatial agreement for some sequences, segmentation similarity remained high, with DSC values ranging from 0.64 to 0.96 for the whole thalamus and its major subdivisions. High within-subject consistency was observed for the whole thalamus (mean DSC = 0.89), while smaller nuclei, such as LD, VM, and MV(Re), exhibited lower DSC values, indicating greater variability across sequences. To our knowledge, no prior studies have specifically examined the spatial similarity of thalamic nuclei segmentations across MPRAGE variants with FastSurfer initialization. Our findings suggest minimal differences in spatial similarity across these MPRAGE variants, particularly when considering the whole thalamus and its major nuclei.

5 | Conclusions

We show the feasibility of automatic thalamic nuclei segmentation with 3T T1-weighted MPRAGE variants using different degrees of CS acceleration in a sample of healthy adults.

Although within-subject thalamic volumes are affected by the choice of sequences, volume variability is low for the whole thalamus and major nuclei, and volume correlations are of appreciable magnitude for the majority of the considered structures. Additionally, the choice of the segmentation tool FastSurfer as initialization point could represent a robust alternative to its counterpart FreeSurfer to further reduce times in the preparation of initialization input for the segmentation of the thalamic nuclei. Our study also shows that, although the effect sizes can be small, the choice of MPRAGE sequence variant matters because it affects the segmentation of thalamic nuclei. This means that in retrospective or prospective MRI studies, attention should be placed to minimizing sequence differences (both within and across MRI sites), or to include these effects as part of the analyses. Further studies are needed to evaluate which are the optimal CS T1w methods for different research

needs, in particular to investigate accuracy and reproducibility of morphometry at the whole-brain level. Studies with a priority for speed and high throughput may prefer CS-MPRAGE with 1- or 2-min acquisitions. On the other hand, studies which allow for longer acquisition times and with an interest in quantitative tissue mapping may opt for CS-MP2RAGE, which provides a T1 map (Mussard et al. 2020).

Based on our evidence, future studies can employ CS-accelerated MPRAGE variants to characterize thalamic nuclei, along with multimodal imaging methods and in different populations, particularly those in which shorter acquisition times are required to reduce the possibility of distortions introduced by high level of motion.

Acknowledgments

This work was supported by funding from the Municipality of the City of Rovereto (Trento), Italy, for the project "Advanced neuroimaging to study aging". Open access publishing facilitated by Universita degli Studi di Trento, as part of the Wiley - CRUI-CARE agreement.

Conflicts of Interest

Tobias Kober and Tom Hilbert are employed by Siemens Healthineers International AG, Switzerland.

Data Availability Statement

Data are available via request to the authors, with the need of a formal data sharing agreement.

References

Alonso, J., D. Pareto, M. Alberich, et al. 2021. "Quantitative Comparison of Subcortical and Ventricular Volumetry Derived From MPRAGE and MP2RAGE Images Using Different Brain Morphometry Software." *Magnetic Resonance Materials in Physics, Biology and Medicine* 34, no. 6: 903–914.

Arend, I., A. Henik, and H. Okon-Singer. 2015. "Dissociating Emotion and Attention Functions in the Pulvinar Nucleus of the Thalamus." *Neuropsychology* 29, no. 2: 191–196.

Bartzokis, G., J. Mintz, P. Marx, et al. 1993. "Reliability of In Vivo Volume Measures of Hippocampus and Other Brain Structures Using MRI." *Magnetic Resonance Imaging* 11, no. 7: 993–1006. https://doi.org/10.1016/0730-725x(93)90218-3.

Baum, G. L., D. R. Roalf, P. A. Cook, et al. 2018. "The Impact of In-Scanner Head Motion on Structural Connectivity Derived From Diffusion MRI." *NeuroImage* 173: 275–286.

Behrens, T. E., H. Johansen-Berg, M. W. Woolrich, et al. 2003. "Non-Invasive Mapping of Connections Between Human Thalamus and Cortex Using Diffusion Imaging." *Nature Neuroscience* 6, no. 7: 750–757.

Benedict, R. H., H. E. Hulst, N. Bergsland, et al. 2013. "Clinical Significance of Atrophy and White Matter Mean Diffusivity Within the Thalamus of Multiple Sclerosis Patients." *Multiple Sclerosis Journal* 19, no. 11: 1478–1484.

Bland, J. M., and D. Altman. 1986. "Statistical Methods for Assessing Agreement Between Two Methods of Clinical Measurement." *Lancet* 327, no. 8476: 307–310.

Blesa, J., I. Trigo-Damas, and J. A. Obeso. 2016. "Parkinson's Disease and Thalamus: Facts and Fancy." *Lancet Neurology* 15, no. 7: e2.

Bloch, L., and C. M. Friedrich. 2021. "Comparison of Automated Volume Extraction With FreeSurfer and FastSurfer for Early Alzheimer's Disease Detection With Machine Learning." In *2021 IEEE 34th International Symposium on Computer-Based Medical Systems (CBMS)*, 113–118. Aveiro, Portugal: IEEE. https://doi.org/10.1109/CBMS52027.2021.00096.

Bocchetta, M., J. E. Iglesias, M. Neason, D. M. Cash, J. D. Warren, and J. D. Rohrer. 2020. "Thalamic Nuclei in Frontotemporal Dementia: Mediodorsal Nucleus Involvement Is Universal but Pulvinar Atrophy Is Unique to C9orf72." *Human Brain Mapping* 41, no. 4: 1006–1016.

Buchsbaum, M. S., T. Someya, C. Y. Teng, et al. 1996. "PET and MRI of the Thalamus in Never-Medicated Patients With Schizophrenia." *American Journal of Psychiatry* 153, no. 2: 191–199.

Byne, W., E. A. Hazlett, M. S. Buchsbaum, and E. Kemether. 2009. "The Thalamus and Schizophrenia: Current Status of Research." *Acta Neuropathologica* 117: 347–368.

de Jong, L. W., K. van der Hiele, I. M. Veer, et al. 2008. "Strongly Reduced Volumes of Putamen and Thalamus in Alzheimer's Disease: An MRI Study." *Brain* 131, no. 12: 3277–3285.

Despotović, I., B. Goossens, and W. Philips. 2015. "MRI Segmentation of the Human Brain: Challenges, Methods, and Applications." *Computational and Mathematical Methods in Medicine* 2015: 1–23.

Dieckmeyer, M., A. G. Roy, J. Senapati, et al. 2021. "Effect of MRI Acquisition Acceleration via Compressed Sensing and Parallel Imaging on Brain Volumetry." *Magnetic Resonance Materials in Physics, Biology and Medicine* 34: 1–11.

Donoho, D. L. 2006. "Compressed Sensing." *IEEE Transactions on Information Theory* 52, no. 4: 1289–1306.

Esteban, O., D. Birman, M. Schaer, O. O. Koyejo, R. A. Poldrack, and K. J. Gorgolewski. 2017. "MRIQC: Advancing the Automatic Prediction of Image Quality in MRI From Unseen Sites." *PLoS One* 12, no. 9: e0184661.

Ferraro, P. M., L. Gualco, M. Costagli, et al. 2022. "Compressed Sensing (CS) MP2RAGE Versus Standard MPRAGE: A Comparison of Derived Brain Volume Measurements." *Physica Medica* 103: 166–174.

Ferris, C. F., J. Tenney, C. Faingold, and H. Blumenfeld. 2013. "Neuronal Networks in Brain Function, CNS Disorders, and Therapeutics." *Functional Magnetic Resonance Imaging in Epilepsy*. https://ur.booksc.eu/book/39528889/6e2e93.

Fiebelkorn, I. C., and S. Kastner. 2020. "Functional Specialization in the Attention Network." *Annual Review of Psychology* 71: 221–249.

Fischl, B. 2012. "FreeSurfer." *NeuroImage* 62, no. 2: 774–781.

Fischl, B., D. H. Salat, E. Busa, et al. 2002. "Whole Brain Segmentation: Automated Labeling of Neuroanatomical Structures in the Human Brain." *Neuron* 33, no. 3: 341–355.

Fisher, R. A. 1936. *Statistical Methods for Research Workers*. 6th ed. New York, NY: Springer.

Friedman, M. 1937. "The Use of Ranks to Avoid the Assumption of Normality Implicit in the Analysis of Variance." *Journal of the American Statistical Association* 32, no. 200: 675–701.

Fujita, N., H. Tanaka, M. Takanashi, et al. 2001. "Lateral Geniculate Nucleus: Anatomic and Functional Identification by Use of MR Imaging." *American Journal of Neuroradiology* 22, no. 9: 1719–1726.

Golden, E. C., J. Graff-Radford, D. T. Jones, and E. E. Benarroch. 2016. "Mediodorsal Nucleus and Its Multiple Cognitive Functions." *Neurology* 87, no. 20: 2161–2168.

Grieve, K. L., C. Acuña, and J. Cudeiro. 2000. "The Primate Pulvinar Nuclei: Vision and Action." *Trends in Neurosciences* 23, no. 1: 35–39.

Griswold, M. A., P. M. Jakob, R. M. Heidemann, et al. 2002. "Generalized Autocalibrating Partially Parallel Acquisitions (GRAPPA)." *Magnetic*

Resonance in Medicine: An Official Journal of the International Society for Magnetic Resonance in Medicine 47, no. 6: 1202–1210.

Guedj, C., and P. Vuilleumier. 2023. "Modulation of Pulvinar Connectivity With Cortical Areas in the Control of Selective Visual Attention." *NeuroImage* 266: 119832.

Hebb, A. O., and G. A. Ojemann. 2013. "The Thalamus and Language Revisited." *Brain and Language* 126, no. 1: 99–108.

Henschel, L., S. Conjeti, S. Estrada, K. Diers, B. Fischl, and M. Reuter. 2020. "Fastsurfer—A Fast and Accurate Deep Learning Based Neuroimaging Pipeline." *NeuroImage* 219: 117012.

Herrero, M. T., C. Barcia, and J. M. Navarro. 2002. "Functional Anatomy of Thalamus and Basal Ganglia." *Child's Nervous System* 18, no. 8: 386–404.

Iglesias, J. E., R. Insausti, G. Lerma-Usabiaga, et al. 2018. "A Probabilistic Atlas of the Human Thalamic Nuclei Combining Ex Vivo MRI and Histology." *NeuroImage* 183: 314–326.

Iglesias, J. E., G. Lerma-Usabiaga, L. C. Garcia-Peraza-Herrera, S. Martinez, and P. M. Paz-Alonso. 2017. "Retrospective Head Motion Estimation in Structural Brain MRI With 3D CNNs." In *International Conference on Medical Image Computing and Computer-Assisted Intervention*, 314–322. Cham: Springer International Publishing.

Jakab, A., R. Blanc, and E. L. Berényi. 2012. "Mapping Changes of In Vivo Connectivity Patterns in the Human Mediodorsal Thalamus: Correlations With Higher Cognitive and Executive Functions." *Brain Imaging and Behavior* 6: 472–483.

Jones, E. G. 2007. *The Thalamus*. 2nd ed. Cambridge: Cambridge University Press.

Kemenczky, P., P. Vakli, E. Somogyi, et al. 2022. "Effect of Head Motion-Induced Artefacts on the Reliability of Deep Learning-Based Whole-Brain Segmentation." *Scientific Reports* 12, no. 1: 1618.

Kendall, M. G. 1948. *Rank Correlation Methods*. Griffin, Oxford University Press.

Keun, J. T. B., E. M. van Heese, M. A. Laansma, et al. 2021. "Structural Assessment of Thalamus Morphology in Brain Disorders: A Review and Recommendation of Thalamic Nucleus Segmentation and Shape Analysis." *Neuroscience & Biobehavioral Reviews* 131: 466–478.

Krishnamoorthy, K., and M. Lee. 2014. "Improved Tests for the Equality of Normal Coefficients of Variation." *Computational Statistics* 29: 215–232.

Landis, J. R., and G. G. Koch. 1977. "The Measurement of Observer Agreement for Categorical Data." *Biometrics* 33: 159–174.

Leszczyński, M., and T. Staudigl. 2016. "Memory-Guided Attention in the Anterior Thalamus." *Neuroscience & Biobehavioral Reviews* 66: 163–165.

Lozano, A. M. 2000. "Vim Thalamic Stimulation for Tremor." *Archives of Medical Research* 31, no. 3: 266–269.

Lustig, M., D. Donoho, and J. M. Pauly. 2007. "Sparse MRI: The Application of Compressed Sensing for Rapid MR Imaging." *Magnetic Resonance in Medicine: An Official Journal of the International Society for Magnetic Resonance in Medicine* 58, no. 6: 1182–1195.

Madan, C. R. 2018. "Age Differences in Head Motion and Estimates of Cortical Morphology." *PeerJ* 6: e5176. https://doi.org/10.7717/peerj.5176.

Magnotta, V. A., S. Gold, N. C. Andreasen, J. C. Ehrhardt, and W. T. Yuh. 2000. "Visualization of Subthalamic Nuclei With Cortex Attenuated Inversion Recovery MR Imaging." *NeuroImage* 11, no. 4: 341–346.

Mair, R. W., L. C. Hanford, E. Mussard, T. Hilbert, T. Kober, and R. L. Buckner. 2019. "Towards 1 Min Brain Morphometry—Evaluating Compressed-Sensing MPRAGE." In *Proceedings of the International Society for Magnetic Resonance in Medicine*, vol. 2019, 2978. Montréal, Canada.

Mair, R. W., L. C. Hanford, E. Mussard, T. Hilbert, T. Kober, and R. L. Buckner. 2020. "Optimizing Rapid Compressed-Sensing MPRAGE Acquisitions for Repeat Sampling of Brain Morphometry Within Individuals." Presented at ISMRM.

Marques, J. P., T. Kober, G. Krueger, W. van der Zwaag, P. F. van de Moortele, and R. Gruetter. 2010. "MP2RAGE, a Self Bias-Field Corrected Sequence for Improved Segmentation and T1-Mapping at High Field." *NeuroImage* 49, no. 2: 1271–1281.

Mönch, S., N. Sollmann, A. Hock, C. Zimmer, J. S. Kirschke, and D. M. Hedderich. 2020. "Magnetic Resonance Imaging of the Brain Using Compressed Sensing–Quality Assessment in Daily Clinical Routine." *Clinical Neuroradiology* 30: 279–286.

Morel, A. 2007. *Stereotactic Atlas of the Human Thalamus and Basal Ganglia*. Boca Raton: CRC Press.

Mueller, S. G., L. Stables, A. T. Du, et al. 2007. "Measurement of Hippocampal Subfields and Age-Related Changes With High Resolution MRI at 4 T." *Neurobiology of Aging* 28, no. 5: 719–726.

Mugler, J. P., III, and J. R. Brookeman. 1990. "Three-Dimensional Magnetization-Prepared Rapid Gradient-Echo Imaging (3D MP RAGE)." *Magnetic Resonance in Medicine* 15, no. 1: 152–157.

Müller, S. J., E. Khadhraoui, N. Hansen, et al. 2023. "Brainstem Atrophy in Dementia With Lewy Bodies Compared With Progressive Supranuclear Palsy and Parkinson's Disease on MRI." *BMC Neurology* 23, no. 1: 114.

Mussard, E., T. Hilbert, C. Forman, R. Meuli, J. P. Thiran, and T. Kober. 2020. "Accelerated MP2RAGE Imaging Using Cartesian Phyllotaxis Readout and Compressed Sensing Reconstruction." *Magnetic Resonance in Medicine* 84, no. 4: 1881–1894.

Najdenovska, E., C. Tuleasca, J. Jorge, et al. 2019. "Comparison of MRI-Based Automated Segmentation Methods and Functional Neurosurgery Targeting With Direct Visualization of the Ventro-Intermediate Thalamic Nucleus at 7T." *Scientific Reports* 9, no. 1: 1119.

Natsume, J., N. Bernasconi, F. Andermann, and A. Bernasconi. 2003. "MRI Volumetry of the Thalamus in Temporal, Extratemporal, and Idiopathic Generalized Epilepsy." *Neurology* 60, no. 8: 1296–1300.

Noor, M. B. T., N. Z. Zenia, M. S. Kaiser, S. A. Mamun, and M. Mahmud. 2020. "Application of Deep Learning in Detecting Neurological Disorders From Magnetic Resonance Images: A Survey on the Detection of Alzheimer's Disease, Parkinson's Disease and Schizophrenia." *Brain Informatics* 7: 1–21.

O'Brien, K. R., T. Kober, P. Hagmann, et al. 2014. "Robust T1-Weighted Structural Brain Imaging and Morphometry at 7T Using MP2RAGE." *PLoS One* 9, no. 6: e99676.

Okubo, G., T. Okada, A. Yamamoto, et al. 2016. "MP2RAGE for Deep Gray Matter Measurement of the Brain: A Comparative Study With MPRAGE." *Journal of Magnetic Resonance Imaging* 43, no. 1: 55–62.

Opfer, R., J. Krüger, L. Spies, et al. 2023. "Automatic Segmentation of the Thalamus Using a Massively Trained 3D Convolutional Neural Network: Higher Sensitivity for the Detection of Reduced Thalamus Volume by Improved Inter-Scanner Stability." *European Radiology* 33, no. 3: 1852–1861.

Pauly, J. M. 2008. "Compressed Sensing MRI." *Signal Processing Magazine, IEEE* 25, no. 2: 72–82.

Power, B. D., and J. C. Looi. 2015. "The Thalamus as a Putative Biomarker in Neurodegenerative Disorders." *Australian and New Zealand Journal of Psychiatry* 49, no. 6: 502–518.

Pruessner, J. C., L. M. Li, W. Serles, et al. 2000. "Volumetry of Hippocampus and Amygdala With High-Resolution MRI and

Three-Dimensional Analysis Software: Minimizing the Discrepancies Between Laboratories." *Cerebral Cortex* 10, no. 4: 433–442.

R Core Team. 2022. *R: A Language and Environment for Statistical Computing*. Vienna, Austria: R Foundation for Statistical Computing. https://www.R-project.org/.

Reuter, M., M. D. Tisdall, A. Qureshi, R. L. Buckner, A. J. van der Kouwe, and B. Fischl. 2015. "Head Motion During MRI Acquisition Reduces Gray Matter Volume and Thickness Estimates." *NeuroImage* 107: 107–115.

Rushmore, R. J., K. Sunderland, H. Carrington, et al. 2022. "Anatomically Curated Segmentation of Human Subcortical Structures in High Resolution Magnetic Resonance Imaging: An Open Science Approach." *Frontiers in Neuroanatomy* 16: 894606.

Schiff, N. D. 2008. "Central Thalamic Contributions to Arousal Regulation and Neurological Disorders of Consciousness." *Annals of the New York Academy of Sciences* 1129, no. 1: 105–118.

Schoonheim, M. M., H. E. Hulst, R. B. Brandt, et al. 2015. "Thalamus Structure and Function Determine Severity of Cognitive Impairment in Multiple Sclerosis." *Neurology* 84, no. 8: 776–783.

Seiger, R., F. P. Hammerle, G. M. Godbersen, et al. 2021. "Comparison and Reliability of Hippocampal Subfield Segmentations Within FreeSurfer Utilizing T1-and T2-Weighted Multispectral MRI Data." *Frontiers in Neuroscience* 15: 666000.

Sherman, S. M. 2017. "Functioning of Circuits Connecting Thalamus and Cortex." *Comprehensive Physiology* 7, no. 2: 713–739.

Sherman, S. M., and R. W. Guillery. 2006. *Exploring the Thalamus and Its Role in Cortical Function*. 2nd ed. Cambridge, Massachusetts, United States: MIT Press.

Shin, K. J., H. J. Lee, and K. M. Park. 2019. "Alterations of Individual Thalamic Nuclei Volumes in Patients With Migraine." *Journal of Headache and Pain* 20: 1–8.

Su, J. H., F. T. Thomas, W. S. Kasoff, et al. 2019. "Thalamus Optimized Multi Atlas Segmentation (THOMAS): Fast, Fully Automated Segmentation of Thalamic Nuclei From Structural MRI." *NeuroImage* 194: 272–282.

Sudhyadhom, A., I. U. Haq, K. D. Foote, M. S. Okun, and F. J. Bova. 2009. "A High Resolution and High Contrast MRI for Differentiation of Subcortical Structures for DBS Targeting: The Fast Gray Matter Acquisition T1 Inversion Recovery (FGATIR)." *NeuroImage* 47: T44–T52.

Sweeney-Reed, C. M., L. Buentjen, J. Voges, et al. 2021. "The Role of the Anterior Nuclei of the Thalamus in Human Memory Processing." *Neuroscience & Biobehavioral Reviews* 126: 146–158.

Tohidi, P., S. Han, L. Zuo, et al. 2023. "Joint Synthesis of WMn MPRAGE and Parameter Maps Using Deep Learning and an Imaging Equation." In *Medical Imaging 2023: Image Processing*, vol. 12464, 558–564. San Diego, California, United States: SPIE.

Tourdias, T., M. Saranathan, I. R. Levesque, J. Su, and B. K. Rutt. 2014. "Visualization of Intra-Thalamic Nuclei With Optimized White-Matter-Nulled MPRAGE at 7 T." *NeuroImage* 84: 534–545.

Tregidgo, H. F., S. Soskic, J. Althonayan, et al. 2023. "Accurate Bayesian Segmentation of Thalamic Nuclei Using Diffusion MRI and an Improved Histological Atlas." *NeuroImage* 274: 120129.

Trotier, A. J., B. Dilharreguy, S. Anandra, et al. 2022. "The Compressed Sensing MP2RAGE as a Surrogate to the MPRAGE for Neuroimaging at 3 T." *Investigative Radiology* 57, no. 6: 366–378.

Van den Heuvel, O. A., G. van Wingen, C. Soriano-Mas, et al. 2016. "Brain Circuitry of Compulsivity." *European Neuropsychopharmacology* 26, no. 5: 810–827.

Van der Kouwe, A. J., T. Benner, D. H. Salat, and B. Fischl. 2008. "Brain Morphometry With Multiecho MPRAGE." *NeuroImage* 40, no. 2: 559–569.

Van der Werf, Y. D., P. Scheltens, J. Lindeboom, M. P. Witter, H. B. Uylings, and J. Jolles. 2003. "Deficits of Memory, Executive Functioning and Attention Following Infarction in the Thalamus; A Study of 22 Cases With Localised Lesions." *Neuropsychologia* 41, no. 10: 1330–1344.

Van Dijk, K. R., M. R. Sabuncu, and R. L. Buckner. 2012. "The Influence of Head Motion on Intrinsic Functional Connectivity MRI." *NeuroImage* 59, no. 1: 431–438.

Vetkas, A., A. Fomenko, J. Germann, et al. 2022. "Deep Brain Stimulation Targets in Epilepsy: Systematic Review and Meta-Analysis of Anterior and Centromedian Thalamic Nuclei and Hippocampus." *Epilepsia* 63, no. 3: 513–524.

Wahl, M., F. Marzinzik, A. D. Friederici, et al. 2008. "The Human Thalamus Processes Syntactic and Semantic Language Violations." *Neuron* 59, no. 5: 695–707.

Wang, F., Y. Lai, Y. Pan, H. Li, Q. Liu, and B. Sun. 2022. "A Systematic Review of Brain Morphometry Related to Deep Brain Stimulation Outcome in Parkinson's Disease." *NPJ Parkinson's Disease* 8, no. 1: 1–11.

Ward, L. M. 2011. "The Thalamic Dynamic Core Theory of Conscious Experience." *Consciousness and Cognition* 20, no. 2: 464–486.

Weeland, C. J., S. Kasprzak, N. T. de Joode, et al. 2022. "The Thalamus and Its Subnuclei—A Gateway to Obsessive-Compulsive Disorder." *Translational Psychiatry* 12, no. 1: 70.

Yarach, U., S. Saekho, K. Setsompop, et al. 2021. "Feasibility of Accelerated 3D T1-Weighted MRI Using Compressed Sensing: Application to Quantitative Volume Measurements of Human Brain Structures." *Magnetic Resonance Materials in Physics, Biology and Medicine* 34: 915–927.

Zacà, D., U. Hasson, L. Minati, and J. Jovicich. 2018. "Method for Retrospective Estimation of Natural Head Movement During Structural MRI." *Journal of Magnetic Resonance Imaging* 48, no. 4: 927–937.

Zhang, D., A. Z. Snyder, M. D. Fox, M. W. Sansbury, J. S. Shimony, and M. E. Raichle. 2008. "Intrinsic Functional Relations Between Human Cerebral Cortex and Thalamus." *Journal of Neurophysiology* 100, no. 4: 1740–1748.

Supporting Information

Additional supporting information can be found online in the Supporting Information section.